Neural encoding of pain uncertainty is selectively amplified when inferring another's pain

L. Loued-Khenissi[1,2], G. A. Bergmann[3,2], C. Corradi-Dell'Acqua[4,2]

1.Department of Clinical Neurosciences, Lausanne University Hospital, Lausanne University

2. Theory of Pain Laboratory, Department of Psychology, Faculty of Psychology and Educational Sciences (FPSE), University of Geneva, Geneva 1202, Switzerland

3. Department of Economics, University of Zurich

4. Center for Mind/Brain Sciences (CIMeC), University of Trento, 38068 Rovereto, Italy.

Abstract

Human social interactions rely on the ability to infer and respond to others' pain, a process inherently subject to uncertainty. Uncertainty is known to shape pain experience and evaluation, yet it is rarely formalized computationally in other-regarding decisions. Here we used a model-based fMRI approach combined with multivariate pattern analyses to examine how expected pain and uncertainty, operationalized as variance-based risk, are represented when decisions concern oneself or another individual. Participants performed a dyadic pain-relief gambling task where pain probabilities and intensities were explicitly defined, enabling trial-wise dissociation of expected pain, risk, prediction error and surprise. Behaviorally, participants showed increased risk aversion, higher valuation of pain relief, and elevated pain ratings when deciding for others. Neurally, we observed a double dissociation: variance-based risk was selectively amplified for others across dorsal striatum and anterior insula, while signed prediction error was more robustly encoded for self. Expected pain was more strongly represented for others, but pain surprise was encoded in anterior insula across targets. Encoding and representational similarity analyses confirmed these patterns, revealing shared representational geometry for prediction errors across targets but stronger voxelwise sensitivity for self. These findings show that 1) a formal uncertainty framework previously applied in other decision domains extends to pain, and 2) that self–other asymmetries in prediction, uncertainty and their associated errors reflect differences in visceral information availability rather than distinct computational architectures.

Significance Statement

When we make decisions about another person's pain, we cannot directly access what they feel: we must infer it under uncertainty. Yet uncertainty in pain research is rarely formalized as a measurable computational quantity. Using model-based fMRI, we show that the brain represents uncertainty about pain as variance-based risk, and that this signal is selectively amplified when pain concerns others rather than oneself. Conversely, prediction error signals are stronger for one's own pain. This double dissociation, amplified uncertainty monitoring but weaker error signals for others, may help explain why caregivers and clinicians misjudge others' pain, and offers a computational framework for understanding how we navigate another's suffering.

Introduction

Uncertainty is a central determinant of how pain is experienced, evaluated, and acted on [3,72,75]. A substantial pain literature has demonstrated that pain perception and pain-related decisions are shaped not only by nociceptive input, but also by expectations, beliefs, and contextual factors [13,53]. Within this literature, uncertainty has long been recognized as influential and has been studied under concepts such as unpredictability, ambiguity, and outcome variability.

However, despite its acknowledged importance, uncertainty in pain research is often treated descriptively rather than formally, limiting the ability to dissociate uncertainty from expected pain, quantify it trial by trial, and examine how it is represented in the brain. In Bayesian and predictive-coding accounts, perception and decision-making are framed as inferential processes in which predictions about outcomes are accompanied by explicit representations of uncertainty [14,31]. From this perspective, other-regarding decisions on pain can be understood as arising from inference over a latent internal state whose value cannot be directly observed but must be estimated from probabilistic cues. These accounts emphasize that predictions are incomplete without uncertainty, as uncertainty governs how expectations are weighted, updated, and translated into behavior. While such computational frameworks have been widely applied to reward-based decision-making and perceptual inference [48,56,67], their systematic application to pain, and particularly to pain concerning others, remains limited.

One formal framework that is especially useful in this context is the mean–variance approach, widely used in decision neuroscience. In this framework, predictions are characterized by the mean of the outcome distribution, while uncertainty is captured by its variance, or risk [43,56,70]. This formulation does not exhaust all possible notions of uncertainty; but it provides a principled and tractable way to dissociate expected pain from uncertainty about pain [4]. Importantly, many pain studies manipulate uncertainty implicitly, for example through unpredictability or cue reliability, without explicitly modeling a separable computational quantity. As a result, it remains unclear whether pain-related inference engages variance-based uncertainty computations analogous to those observed in other decision domains.

Inferring another's pain is uniquely challenging, as the state cannot be accessed through sensory systems [37] and thus depends on indirect cues [5]. When deciding for others, uncertainty is amplified by bias, social distance and lack of shared embodiment [44], [52]. Understanding how we navigate uncertainty is crucial where individuals act as surrogate decision-makers[52], [17]: clinical studies show that clinicians and caregivers routinely underestimate patients' pain [30,59,61]. From a computational perspective, such misestimation may arise not only from differences in expected pain, but from differences in how uncertainty is assessed or weighted when internal states must be inferred in others.

If uncertainty about outcomes is formally represented as variance-based risk, and inferring another's pain necessarily increases uncertainty, then vicarious pain provides a critical test case for computational accounts of pain inference. Decision-making under uncertainty is well studied for oneself [45,73], for others in reward domains [66], but uncertainty's effect on vicarious pain remains poorly understood [39]. In monetary decisions, uncertainty promotes risk aversion for gains and risk-seeking for losses[29], a pattern extending to pain and disease [38]. Uncertainty provokes risk-seeking when deciding for others [54], though this may not generalize to pain[40]. Unpredictability amplifies own pain perception[15,78]. Critically, most prior work has operationalized uncertainty implicitly, without explicitly formalizing or dissociating expected pain from outcome variance as separable computational quantities. Two studies explicitly dissociated expected pain from uncertainty in vicarious pain, reporting mixed findings [76], [78]. Whether uncertainty itself is encoded as a formal risk signal during pain inference, and whether this signal is differentially weighted for others' pain, therefore remains an open question.

Neuroimaging studies on decision-making under uncertainty implicate the striatum [32,56,70] and anterior insula [28,47,58,66,68]. Their role spans domains [41], making them prime candidates for pain-related inference. In particular, work in the reward domain has demonstrated a dissociation between striatal encoding of expected value and risk, establishing dorsal striatal responses as a neural signature of variance-based uncertainty. The anterior insula, in particular, is repeatedly implicated in pain processing [16,19,27,42,46] and in signaling uncertainty, including risk [58]. Testing whether these domain-general uncertainty signals extend to pain allows us to ask whether similar computational variables are recruited when decisions concern an inferred internal state rather than an external

outcome. Investigating whether theses computations differ for self versus other will clarify whether individuals rely on shared inferential principles [2,22] when making pain-related decisions for themselves and for others.

In this study, we examined how uncertainty affects pain-related decision-making for self and others, formalizing inference through expected pain (mean), risk (uncertainty), and prediction errors. Participants performed a decision-making task during fMRI, making choices to mitigate threatened pain through a lottery and a wager. Uncertainty was introduced via probabilistic visual cues, enabling trial-wise estimation of predictive variables. Trials were presented in two blocks targeting self-pain and other-pain. By dissociating expected pain from risk, we tested whether social context selectively modulates uncertainty weighting during pain inference. This approach allowed us to ask whether variance-based risk signals observed in other domains extend to pain, and critically, to pain concerning others. We hypothesize that (1) neural representations of predicted pain scale with expected value and risk in both targets, recruiting the same regions (striatum, anterior insula) implicated in reward-based inference; and (2) the striatum and anterior insula respond to trial-wise values of risk and prediction errors [3,21,50]. We further explored whether self-other differences emerge at distinct stages of the inference process, specifically whether predictive computations (expectation, uncertainty) and prediction updates (prediction error, surprise) are differentially engaged across targets.

Results

Of 36 participants, 3 were excluded (2 for calibration errors, 1 for coil misplacement), leaving 33 deciding agents (13 male; mean age 23.2 ± 4.3 years) in 33 dyads.

Behavioral Results

A Prelec probability weighting model based on individual bids offered for pain relief yielded subjective values that were then compared to objective task-derived regressors, confirming the latter were appropriate for analysis (SI Appendix).Three GLME models revealed a consistent pattern of heightened risk aversion for others. Expected pain ($t = 2.23$, $p = .026$), risk ($t = 2.54$, $p = .011$), and target identity ($t = 2.64$, $p = .008$) predicted sure-option selection (Model 1). Bids were driven by expected pain ($t = 7.98$, $p < .001$) and risk ($t = 2.96$, $p = .003$), with marginally higher bids for others ($t = 1.85$, $p = .065$) and a significant EP × target

interaction ($t = 3.62$, $p = .003$) (Model 2). Pain ratings showed inflated estimates for others' pain ($t = 3.51$, $p = .005$), with no effect of prediction errors on ratings (Model 3; Figure 1).

Taken together, results suggest a differential pattern of choice behavior for a pain threat to another, in the form of heightened risk aversion in both models 1 and 2, higher pain relief valuation for the other in Model 2, and inflated pain ratings in model 3 (Figure 1). A direct effect of uncertainty (risk) on decision-making was only found in the prediction phase of the decision and neither prediction errors affected subjective pain ratings.

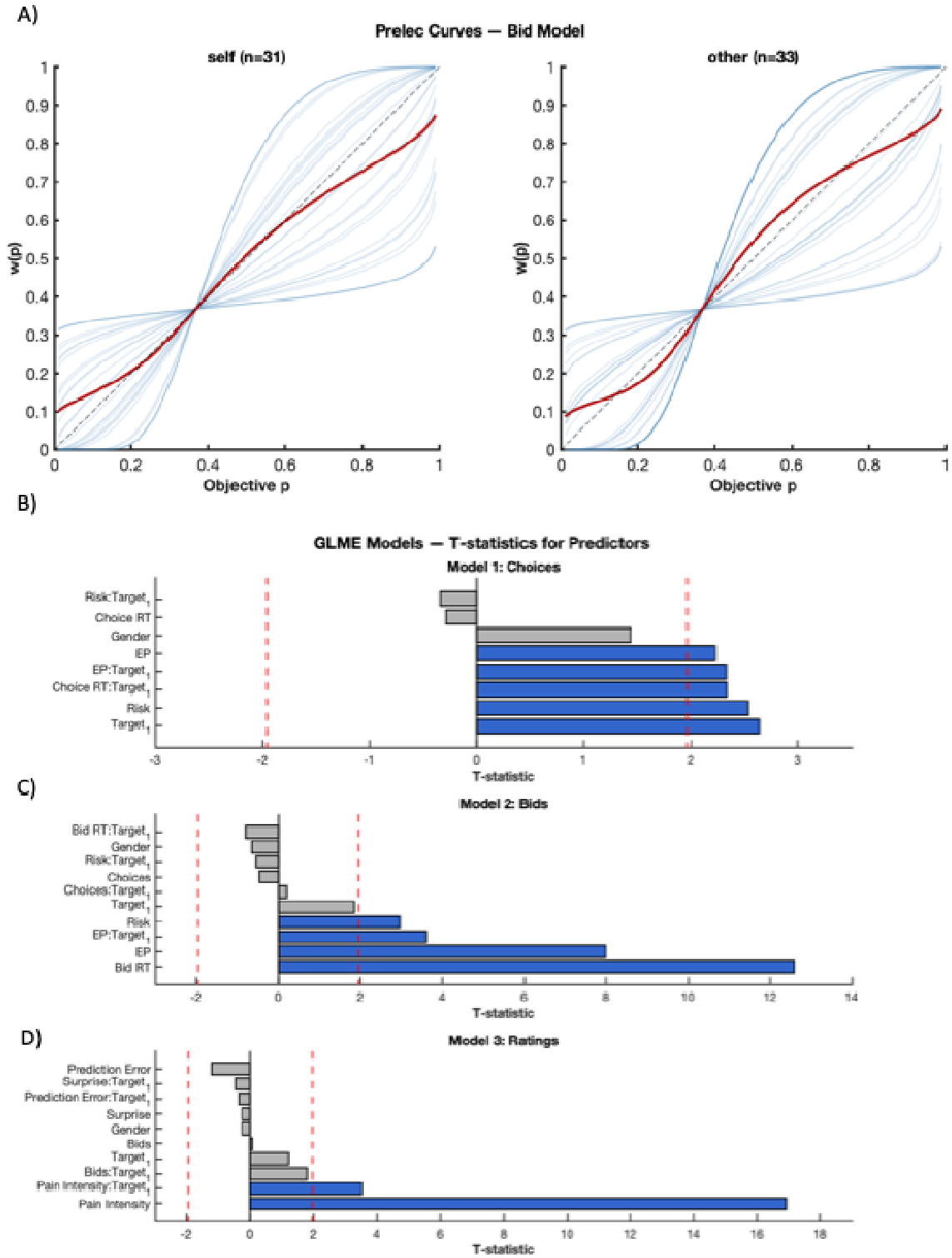

Figure 1 Behavioral results and computational modeling of pain inference. A) Subjective probability weighting (Prelec). Estimated Prelec functions () mapping objective probabilities to subjective decision weights for Self

and Other conditions. T-statistics for fixed-effect predictors from three generalized linear mixed-effects (GLME) models: (B) choice behavior, (C) bid value, and (D) pain intensity ratings. Each horizontal bar reflects the t-statistic for a fixed-effect term; red dashed lines mark approximate significance thresholds (|t| > 1.96). The x-axis is scaled dynamically to reflect the range of t-values, with the left bound fixed at –3.

Neuroimaging Results

Predicted pain is more strongly represented for others

Expected pain for other elicited FWE-corrected whole-brain responses in visual cortex (cuneus, fusiform; peak T = 7.37) and cluster-corrected responses in supplementary motor cortex/mid-cingulate. No whole-brain effects survived for self..

Beta extraction within ROIs revealed an inverse pattern for self-pain: expected pain betas were significantly negative in bilateral ACC (left: t(32) = -2.95, p = .006; right: t(32) = -2.61, p = .014), consistent with a valuation-based framing in which decreasing expected pain tracks increasing distance from a negative outcome. Paired self-vs-other comparisons confirmed stronger EP representation for other in left ACC (t(32) = -2.08, p = .046) and left caudate (t(32) = -2.34, p = .026).

Multivariate analyses provided converging evidence for EP representations. The encoding model detected significant negative EP encoding for self in left caudate (Fisher-z = -0.095, p = .015), consistent with the negative beta values observed in the univariate analysis and with a valuation-based framing in which lower expected pain tracks proximity to a favorable outcome. Self-vs-other encoding differences were significant in left caudate (p = .042). RSA revealed a trend toward structured EP representational geometry for other in left caudate (r = 0.035, p = .067), with a trend-level self-vs-other difference (p = .036). Together, these results indicate that expected pain representations are more strongly structured for others, while self-related EP signals in cingulate and caudate show an inverse, valuation-consistent pattern.

Uncertainty encoding is selectively amplified for others' pain

The most striking self-other dissociation emerged for pain risk. No whole-brain FWE-corrected responses survived for risk in either condition, though extensive cluster-corrected activation was observed for both self (20 clusters) and other (20 clusters, with the largest spanning 19,279 voxels centered on right thalamus for other). SVC analysis showed robust

risk encoding for the other in all key uncertainty-processing regions: bilateral putamen (left: T = 5.28, p(FWE) < 0.001, [-22, 2, 8]; right: T = 5.37, p(FWE) < 0.001, [28, -6, -4]), bilateral caudate (left: T = 4.58, p(FWE) = .004, [-14, 2, 18]; right: T = 4.69, p(FWE) = .003, [18, 2, 16]), and bilateral anterior insula (left: T = 3.96, p(FWE) = .025, [-44, 4, -6]; right: T = 3.86, p(FWE) = .031, [36, 6, 4]). For self, risk reached significance only in left caudate (T = 3.97, p(FWE) = .017, [-16, 18, 12]) (Table 3).

Beta extraction explicitly supports this pattern. Risk for the other was significant in all six anatomical ROIs: bilateral anterior insula (left: t(32) = 3.21, p = .003; right: t(32) = 2.32, p = .027), bilateral caudate (left: t(32) = 2.96, p = .006; right: t(32) = 2.47, p = .019), and bilateral putamen (left: t(32) = 3.73, p < .001; right: t(32) = 3.42, p = .002). No ROI showed significant risk encoding for self at the beta level. Self < other differences were significant in right anterior insula (t(32) = -2.36, p = .025) and bilateral putamen (left: p = .039; right: p = .036) (Table 4).

Multivariate analyses converged with the univariate findings. The encoding model detected significant risk encoding for other in seven ROIs: left ACC (z = 0.069, p = .031), bilateral anterior insula (left: z = 0.057, p = .046; right: z = 0.067, p = .038), bilateral caudate (left: z = 0.079, p = .017; right: z = 0.067, p = .041), and bilateral putamen (left: z = 0.084, p = .006; right: z = 0.078, p = .011). No significant risk encoding was detected for self. Self-other encoding differences were significant in right putamen (p = .029), with a trend in right anterior insula (p = .059). RSA revealed a significant self-other difference in right ACC (p = .025), though no individual-condition RSA effects reached significance. The convergence across SVC, beta extraction, and encoding model provides robust evidence that risk encoding during pain inference is selectively amplified for others across dorsal striatum, anterior insula, and cingulate cortex.

Signed prediction error encoding is stronger for self than other

In contrast to the other-dominant pattern observed for risk, signed prediction error (PE) showed stronger encoding for self. Beta extraction yielded a significant PE effect for self in left caudate (t(32) = 2.12, p = .041), with a significant self > other difference (t(32) = 2.22, p = .034). No other univariate PE effects reached significance.

Multivariate analyses strongly confirmed and extended this pattern. RSA revealed that bilateral anterior insula carried significant representational information about signed PE for both self (left: $r = .059$, $p = .004$; right: $r = .068$, $p = .003$, 7/33) and other (left: $r = .054$, $p = .003$; right: $r = .048$, $p = .011$), as well as right caudate for both targets (self: $p = .019$; other: $p = .021$). Self-vs-other RSA differences were not significant for PE in any ROI, indicating that the representational geometry of prediction errors was shared across targets.

The encoding model, however, revealed a striking quantitative dissociation. Signed PE was robustly encoded for self across the following ROIs: bilateral anterior insula (left: Fisher-z = .291, $p < 10^{-7}$; right: $z = .317$, $p < 10^{-7}$), bilateral caudate (left: $z = .120$, $p = .010$; right: $z = .119$, $p = .009$), right ACC ($z = .124$, $p = .024$), and bilateral putamen (left: $z = .161$, $p = .004$; right: $z = .124$, $p = .029$). Encoding was also significant for other, but substantially weaker, reaching significance only in bilateral anterior insula (left: $z = .100$, $p = .030$; right: $z = .126$, $p = .006$). Critically, self > other encoding differences were significant in bilateral anterior insula (left: $p = .007$; right: $p = .009$), bilateral caudate (left: $p = .006$; right: $p = .013$) and left putamen ($p = .048$). This pattern suggests that direct nociceptive experience generates a more precise prediction error signal than vicarious inference, consistent with the view that first-person pain provides higher-fidelity sensory input for updating internal models.

Anterior insula encodes pain surprise for both self and other

Pain surprise evoked responses in the right anterior insula for both self and other, localized within a region previously identified as encoding domain-general surprise (Loued-Khenissi et al., 2020). Pain surprise evoked SVC-significant responses in right anterior insula for both self ($T = 3.90$, $p(FWE) = .016$) and other ($T = 3.43$, $p(FWE) = .039$), localized to a previously identified domain-general surprise region [43]. Beta extraction confirmed this pattern (both $p < .05$). No significant self-vs-other differences were observed. The encoding model detected surprise encoding for self in left anterior insula ($z = .097$, $p = .032$) but not for other; RSA did not detect significant surprise effects. These results indicate a common anterior insula mechanism across targets.Taken together, these results indicate that pain surprise engages a common anterior insula mechanism across targets, consistent with a domain-general uncertainty signal.

Figure 2. Expected Pain and Risk (Predictive Phase)

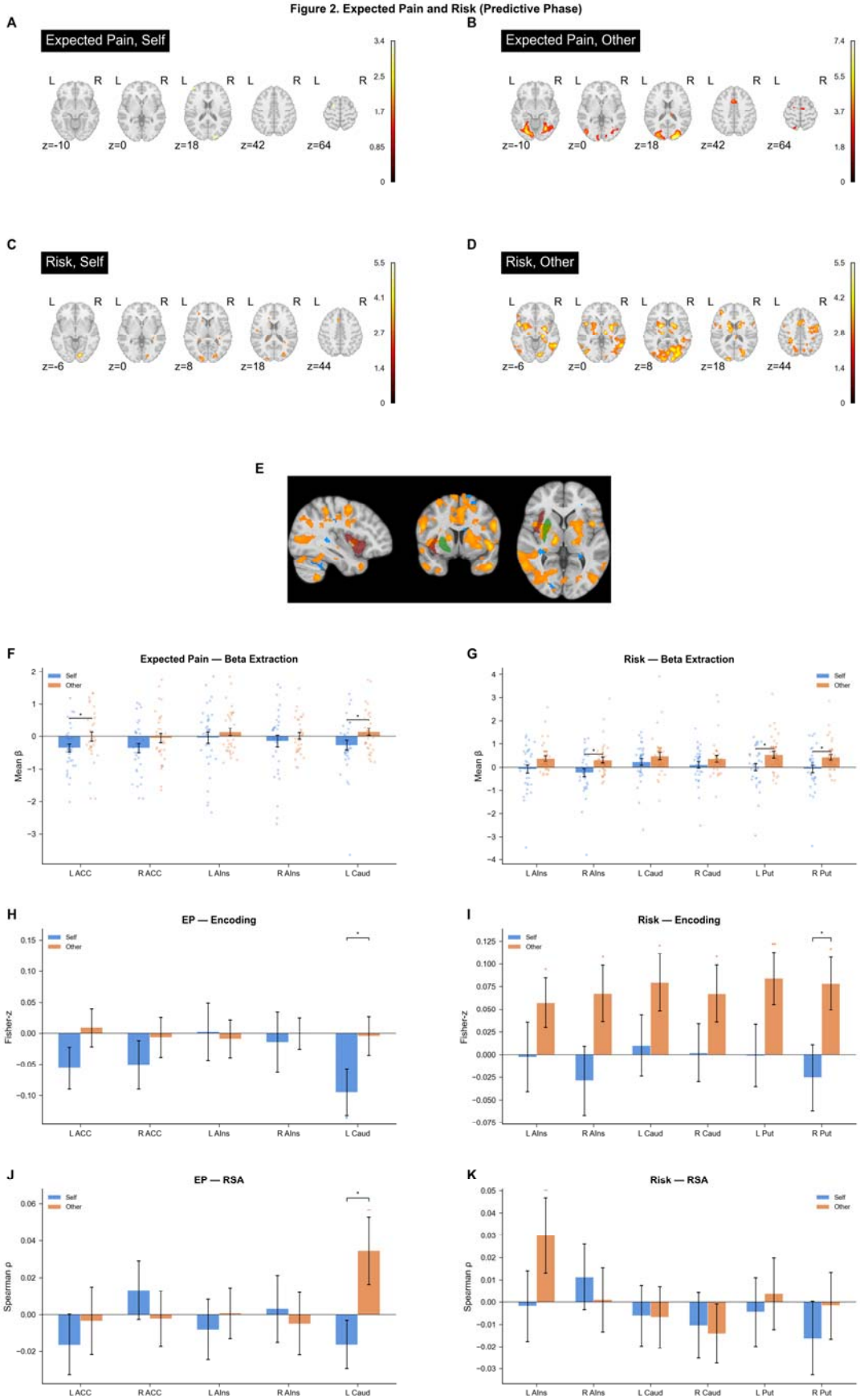

1

Figure 2. Neural correlates of Expected Pain (EP) and Risk during the predictive phase. (A-D) Whole-brain univariate activation maps for EP and Risk, split by target (Self vs. Other), displayed in MNI space. Maps are thresholded at $p < 0.005$ (uncorrected) with a cluster-extent threshold of $k = 25$ for visualization. Dots represent individual subjects; error bars indicate SEM. (H-I) Multivariate encoding model results (Fisher-z) (J-K) Representational Similarity Analysis (RSA, Spearman rho) * $p < 0.05$, ** $p < 0.01$, *** $p < 0.001$, ~ $p < 0.10$.

Figure 3. Prediction Error and Surprise (Post-Outcome Phase)

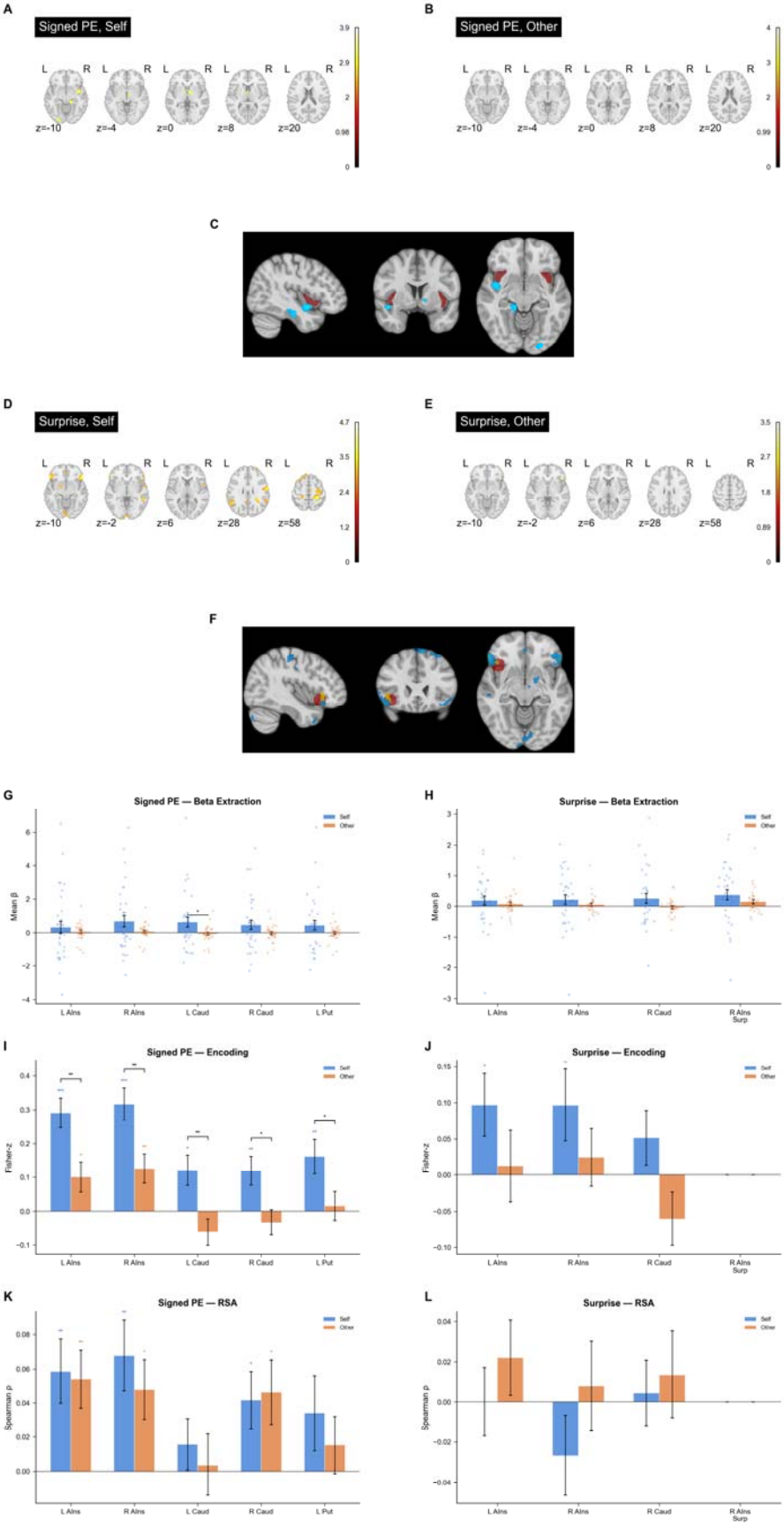

1

Figure 3. Neural correlates of Signed Prediction Error (PE) and Surprise during the post-outcome phase. (A-B) Univariate activation maps for Signed PE (C) ROI detail for PE. (D-E) Univariate maps for Surprise. (F) ROI detail for Surprise, within a domain-general surprise sphere. All maps thresholded at $p < 0.005$ (uncorrected), $k = 25$. (G-H) Mean parameter estimates (beta extraction) confirming significant PE encoding for Self in left caudate ($p = .041$) and common surprise encoding in the right anterior insula sphere for both targets. (I-J) Multivariate encoding model results (K-L) RSA results Error bars represent SEM; dots represent individual subjects. * $p < 0.05$, ** $p < 0.01$, *** $p < 0.001$, ~ $p < 0.10$.

Summary of neuroimaging findings

These findings address two hypotheses. First, consistent with the prediction that pain inference conforms to domain-general predictive coding principles, all four computational variables (expected pain, risk, prediction error, and surprise) were encoded in regions previously implicated in reward-based inference under uncertainty, including dorsal striatum, anterior insula, and ACC. Pain surprise was localized to the same anterior insula region previously reported for perceptual and economic surprise, providing direct evidence for a shared computational architecture across domains.

Second, the self-other comparison reveals a structured dissociation across stages of the inference process. Expected pain and variance-based risk are amplified for others, primarily in visual cortex, cingulate, dorsal striatum, and anterior insula, with risk encoding for the other constituting the study's strongest and most consistent finding. Signed prediction error, though represented for both targets in RSA, is more robustly encoded for self across anterior insula, caudate, and putamen in the encoding model, reflecting a stronger response to learning from direct nociceptive experience. Pain surprise, by contrast, is encoded in right anterior insula for both self and other without significant target differences, supporting a domain-general signal that operates independently of whether pain concerns oneself or another. Pain intensity and rating results are reported in the Supplementary Materials.

Discussion

Uncertainty plays a fundamental role in decision-making, yet its neural implementation in the context of pain remains poorly understood [12,24,65,69]. Our study examines how uncertainty, formalized as variance-based risk, is incorporated into inference and decision-making when decisions about pain concern oneself or another individual. We tested two hypotheses. First, that pain inference for self and other conforms to domain-general predictive coding principles, recruiting the same computational variables (expected value, risk, prediction error, surprise) in neural substrates identified in reward-based decision-making. Second, that the self-other distinction in pain produces differential engagement

across stages of the inference process: expectation, expected uncertainty, error on expectation (signed prediction error) and error on uncertainty (surprise). Our findings support both hypotheses and unveil a structured dissociation organized around embodiment. Specifically: 1) pain expectation is amplified for others in visual and cingulate cortices; 2) variance-based risk encoding is selectively amplified for others across dorsal striatum and anterior insula, constituting the study's strongest finding; 3) signed prediction error, the only variable reflecting direct nociceptive input, is more robustly encoded for self; and 4) pain surprise is shared across targets in the same anterior insula region previously reported for perceptual and economic surprise[41]. Together, these results outline a double dissociation: prior-dependent computations (expectation and uncertainty) are amplified for others, while outcome-dependent updating (prediction error) is amplified for self, with surprise serving as a domain-general update signal that operates independently of whose pain is at stake.

Risky decision-making for others

Behavioral results on decision-making for others' pain largely replicate previous findings [39], revealing a consistent pattern of risk aversion when deciding for others, in contrast to reports of equal or increased risk-taking in other-regarding monetary decisions [54]. As in our earlier work, we observed a higher monetary valuation of others' pain relief compared to one's own, and an overestimation of others' pain intensity, suggesting a cautious approach to vicarious pain evaluation, in contrast to reported underestimation in clinical settings [30,59,61]. Reaction times indicated increased deliberation for others' decisions, a hallmark of higher uncertainty [9]. More risk-averse, costlier decisions may point to altruistic motivations previously found in other studies [6,20,26] but we propose that other-regarding behaviors may instead reflect a drive to minimize uncertainty introduced by the agent's lack of direct access to the target's internal state. Taken together, behavioral differences between self and other decisions suggest differences in uncertainty weighting applied to similar internal models, rather than fundamentally distinct decision processes.

Mental representation of expected pain and its risk, in self and other

From a computational inference perspective, pain anticipation should involve a mental representation of the expected stimulus and its associated uncertainty. Significant positive responses to trial-by-trial expected pain for the other in visual areas (occipital and fusiform gyri), the cuneus and the cingulate (regions previously implicated in both self- and vicarious pain [35]) reflect a graded neural representation of predicted vicarious pain. The visual cortex

activation might reflect attentional processing of cues related to the other's potential pain [8,74], while mid-cingulate involvement could indicate a predictive modeling of the anticipated sensory consequences for the other [34,64]. Interestingly, we did not observe a similar positive neural response to one's own expected pain. Instead, we found significant **negative beta values in** the anterior cingulate, implicated in anticipated negative outcomes [49] including pain avoidance [60]. This asymmetry may suggest a differential framing of self-versus-other pain: for others, pain is punishment, and no-pain, zero; but for one's self, pain is zero and no pain, *reward* [71]. Multivariate analyses confirmed this pattern: the encoding model detected significant negative EP encoding for self in caudate, while RSA showed a trend toward structured EP representations for others in the same region, with a significant self-vs-other difference. This convergence across methods suggests that expected pain engages similar regions for both targets but with opposite computational signatures.

We further find significant neural responses to pain risk decoupled from pain expectation, across all key uncertainty-processing regions examined: bilateral anterior insula, bilateral caudate, and bilateral putamen, as well as the dorsal striatum, highlighted as the most reliable region in test-retest studies on decision-making under risk [33]. Striatal and insular responses to pain risk were selectively amplified when decisions concerned others, paralleling behavioral risk aversion in vicarious contexts.

Enhanced neural engagement for other-risk may reflect compensation for greater uncertainty in inferring another's internal state. The encoding model independently confirmed this pattern, detecting significant risk encoding for other but no significant effects for self. The selective amplification of risk for others is consistent with the interpretation that, lacking direct sensory access to the other's pain state, the brain compensates by increasing the weight placed on expected uncertainty.

Pain, prediction and error

Signed prediction error showed the inverse pattern to risk: encoding was stronger for self than other. RSA identified PE representations in bilateral anterior insula for both self and other, indicating shared representational geometry across targets. The encoding model, however, revealed a striking quantitative dissociation: PE was encoded for self across most of the ROIs examined (bilateral anterior insula, caudate and putamen,), with self > other differences significant in most regions examined. Signed PE is the only computational

variable in our framework that requires direct nociceptive information: it is defined as the difference between actual pain outcome and expected pain. The self-dominance of PE encoding may thus not be incidental but reflect a fundamental constraint of vicarious inference: visceral information yields the generation of a signed error signal and does not emerge when one has not physically experienced that state. The finding that RSA detects shared PE geometry while the encoding model detects self-dominant sensitivity is informative: it suggests that self and other pain recruit the same representational structure but with different signal-to-noise, rather than engaging qualitatively distinct computations.

By contrast, across both self and other targets, surprise evoked a response in the right anterior insula, consistent with prior work on surprise across domains [41] and pain inference [11,19,23,62,63],[25]. Importantly, these surprise responses were localized to the same constrained region previously reported for both perceptual and economic surprise, supporting the idea of a common computational mechanism in the anterior insula that signals update on expected uncertainty, irrespective of outcome quality, nature or function. No significant self-vs-other differences were observed for surprise, consistent with a domain-general signal that detects the magnitude of deviation from expectation regardless of whose pain is at stake. This is notable because surprise, unlike signed prediction error, does not encode the direction of the error and therefore does not require information about the actual pain state. Its invariance across targets is thus consistent with the broader pattern in which computations that depend on embodied information (signed PE) show self-dominance, while those that can be computed from external cues alone (surprise, risk) do not.

The complementary patterns observed for risk and prediction error constitute a double dissociation: uncertainty monitoring is amplified for others, while signed error-driven updating is amplified for self. This asymmetry is consistent with a computational account in which vicarious inference, lacking direct sensory access to another's internal state, compensates by increasing the weight placed on prior uncertainty (risk) while generating weaker posterior updates (prediction error). Such a pattern aligns with Bayesian accounts in which reduced sensory precision for others leads to greater reliance on the prior.

Applications and Implications

Our results have several implications. First, we identify costly other-regarding tendencies when individuals decide about another person’s pain. This pro-sociality may be motivated by

a desire to attenuate pain in another [77]; to reduce uncertainty during inference [40]; or to conform to social norms [51] under observation [1]. Regardless of motivation, participants consistently prioritized others' pain over economic gain. Second, these findings suggest that decisions about self and other rely on partially distinct processes, consistent with the view that inference about others' internal states cannot be reduced to simple simulation [2]. At the same time, shared encoding of surprise supports common inferential mechanisms across targets.

Beyond basic decision-making, these findings are relevant to contexts in which individuals act as surrogate decision-makers for pain. Although others' pain is often underestimated in clinical settings, in contrast to the cautious overestimation observed here, both patterns may reflect differences in how uncertainty is weighted under constrained information. The double dissociation we observe, amplified risk but weaker signed prediction errors for others, offers a computational account for this clinical pattern: decision-makers may over-weight uncertainty about others' pain while under-updating from outcome feedback, but not on learning to reduce uncertainty, the purpose of the surprise signal. By situating these results within broader work on prediction and pain, our findings add to evidence that uncertainty plays a central role in shaping pain-related judgments.

Limitations

The study is not without limitations. In our study, agents do not employ such cues as targets' facial expressions[7], vocalizations[36] or declarations[10], unlike our previous study, where agent and target were seated together, conveying additional information to the decision-maker. This difference in context may prove critical to further studying the effects of uncertainty on assessing others' pain. At the same time, as decisions made in our study were blind and disembodied, they can be simulated by an artificial agent that, in the future, may provide guidance on clinical decision-making in pain given established statistical parameters (probability of pain, expected pain risk and unexpected pain outcomes).

Conclusions

In this study, we provide evidence for a neurally instantiated, graded representation of another's expected pain and for selective amplification of uncertainty encoding when pain concerns others, demonstrating an intrinsic, computational mechanism for vicarious pain processing that integrates uncertainty when facing potential harm. By employing model-based fMRI and multivariate pattern analyses, we show the critical role of uncertainty in shaping how we perceive and respond to the pain of others, offering a direct comparison with our own pain processing. We further demonstrate that prediction error encoding is stronger for self, revealing a double dissociation between uncertainty and error that reflects differences in information availability across targets. The organizing principle is embodiment: computations that depend on direct sensory access to the pain state are amplified for self, while those computable from external cues are amplified for others. This work expands the applicability of computational models of inference to how we navigate another's suffering, with implications for understanding clinical contexts in which surrogate decision-makers must act under irreducible uncertainty about another's pain.

Methods

Population

The study was conducted at the Campus Biotech in Geneva, Switzerland. A total of 72 participants (36 dyads) enrolled in the study. Sample size was comparable to prior model-based fMRI studies on uncertainty (n≈25–35). Participants were recruited from both the University of Geneva Campus and the general population. Inclusion criteria included: French-speaking; 18 -45 years of age; and good general health. Exclusion criteria included: reported psychiatric or neurological diagnoses; current or recent psychotropic drug use; claustrophobia; metal or other implants that may interfere with the MR scanner. Study information, including the task procedure and MR safety guidelines, was sent electronically to all participants 2 days before the scheduled experiment session. Upon arrival at the study center, participants were given paper versions of the information and consent forms. Participants were asked to read these, confirm their understanding of the study’s risks and benefits, and sign the forms before continuing with the experiment. Following intake, the experimenter verbally explained the study structure and task process. Once participants understood the experiment, they were each randomly assigned a fixed role in the task: they

were either cast as a Deciding Agent (DA), or a Passive Recipient (PR). The DA's role in the experiment was to enter the scanner, and make decisions both for herself and the PR. The PR's role was to act as the recipient of half of the DA's decisions. The study was approved the Commission Cantonal d'Ethique de la Recherche sur L'Etre Humain in December, 2019. Data collection was conducted between April and July, 2021.

Of the 36 participants enrolled as deciding agents (DAs) in the study, 2 were excluded from analysis because laser fluence levels for the hand (which are lower in energy range) were erroneously used on their ankles, resulting in a lack of perceived pain. An additional participant was excluded from analysis due to a misplacement of the MR head coil, resulting in only half of the coils receiving signal. The remaining participant pool comprised 33 DAs (13 Male; average age, 23.22 years, sd = 4.33) participating in 33 dyads. Efforts were made to counterbalance DA sex when possible, alternating between males and females, but the participant pool consisted mostly of women. Twelve dyads consisted of agents of different sex across the dyad. Mean payout was 17.28 CHF (sd = 3.65). Of the 33 participants, 5 consistently made the same choice for themselves across trials; of these, 3 always gambled and 2 always selected the sure option. Two participants (one of which was also one of the 5 consistent self gambles) always selected the same option for the other (1 gambler and 1 fully risk averse). Finally, 2 participants made no bids in the self condition. All participants bid > CHF for the other condition.

Procedure

Following intake, both participants were asked to remove metallic items and leave personal affairs in dedicated lockers before being led to the scanner control room. Here, both participants were briefly shown the laser pain stimulation machine and the PR was asked to take a seat in the control room. Once in the scanner room, they were given earplugs and MR compatible headphones. Several sensors were fitted on the DA, including a pulsemeter to record cardiac signals; a pneumatic sensor around the waist to measure respiration; and two electrodes on 2 of the left-hand fingers, to record skin conductance. Before placing the coil, DAs were shown the button response box on which they were to provide their answers. They were then moved into the scanner to begin image acquisition. Finally, a laser-safe cloth was draped over the opening of the bore, to ensure that, in case a laser emission went astray, it would not harm the participant.

While DAs were being prepared for scanning, they were led to believe that PRs were undergoing a pain calibration procedure in the MRI control room. In reality, no such procedure was performed, as laser pain stimulation could not be administered in the control room due to safety constraints related to its glass walls at the Fondation Campus Biotech in Geneva. Consequently, a deception was introduced whereby DAs believed that PRs would be the recipients of pain on half of the task trials and therefore required calibration. After DAs were positioned in the scanner and the initial MR localizer sequence was launched, PRs were paid 30 CHF, fully debriefed, and dismissed. DAs were informed at the end of the experiment that PRs had not received pain; throughout the task, all DAs believed that a real person was present and potentially affected by their decisions.

MRI acquisition

Scans were acquired in a 3T Siemens MRI scanner located at the Campus Biotech MRI platform. Sequences during the study were acquired as follows: a field-map scan (2D GR TR=677ms/TE=4.92ms/FA=60deg/SO=PFP); two functional scans of about 20 mins each ([112 112 72], 2D EP TR=1100ms/TE=32ms/FA=50deg, Mosaic Multi-band) where the task was administered; a T1-weighted anatomical scan ([256 256 208], 3D GR\IR TR=2200ms/TE=2.96ms/FA=9deg/SO=IR\PFP).

Pain Calibration Procedure

The experimental task required 3 levels of pain (low, medium and high) to be made available to the decision target. Because pain is a subjective experience, we performed a calibration procedure on the DA, following their field map scan acquisition and prior to starting the task. This calibration procedure consisted of stimulating the area around the DA's ankle bone, as this body part was 1) accessible to the experimenter; 2) glabrous skin. Pain stimulations were evoked via nociceptive radiant heat stimulation using an infrared neddymium: yttrium-aluminium-perovskite laser system (Nd: YAP; Stimuli 1340; El. En, Florence; lambda = 1340 nm; pulse duration, 4 ms; beam diameter 6 mm^2). The wand of the laser stimulation was passed through an opening in the wall separating control and MR rooms to allow the experimenter to administer stimulations on the DA during functional scans. Stimulations at energies of 1.5-3 J were emitted randomly in step intervals of .25 J, three times each. After each stimulation, DAs rated the pain experienced on a scale presented on the in-bore screen using the button response box. The scale ranged from to 10, with indicating no pain, and 1 a first pain, and 10 representing maximum pain, consistent with our previous research[40].

Responses for each energy level were then averaged such as to obtain a low, medium and high pain level (average ratings closest to 1; 5 and 9, respectively). In cases where a pain level was equal to another, an additional .25 J was added to the higher pain level. Once individual pain levels were computed, the 3 pain levels were presented to the DA once more, to ensure the participant knew which pain corresponded to their assignation of low, medium and high levels. During the calibration and the task, all parties present were required to wear laser safety goggles. The only exception was the DA whose upper half of the body was protected by laser-safe curtains certified for the wavelength of the stimulator.

Task procedure

DAs performed two blocks of 18 trials of a decision-making task in the scanner. At each block, participants started off with an endowment of 216 monetary units (MUs), equivalent to 21.6 CHF. At each trial, DAs were first presented with a visual cue, depicting a probability (in the form of a red pie chart on a grey background), and an intensity (represented by 2 or 3 red lightning bolts) of threatened pain, for 6 seconds (Figure 4B). Probabilities ranged from .1-0.9 in steps of .1. DAs were then given 6 seconds to either gamble to avoid the pain altogether, with a 50% chance of winning; or select a sure option, where, if pain were the outcome, it would certainly be reduced by one level. Participants that did not respond in time incurred a penalty of 10 MUs. In the next screen, participants were asked to bid on their decision, selecting a price that ranged from -10 MUs on a scale. Participants that did not respond in the allotted 6 s entered a default “0” for their bid. DA bids were then compared to a hidden reserve price randomly selected for each trial. Bids matching or exceeding this reserve price were accepted as purchase prices for the initial decisions, and the latter were applied to initial values of expected pain, while rejected bids left the DA facing the initial probability and intensity of threatened pain. The bid status (accepted or rejected) was presented on the screen for 6 seconds. Finally, pain was delivered depending on resultant probabilities and intensities. A visual cue representing this pain delivery was simultaneously presented on the in-bore screen, as either initial values of pain intensity (2 or 3 red lightning bolts); reduced values of pain intensity (2 or 3 yellow lightning bolts) or no pain (3 greyed out lightning bolts). In no pain trials, DAs received a non-painful laser stimulation of .5 J. The outcome screen was presented for 6 seconds. Finally, DAs were asked to rate the pain outcome on a visual rating scale, this time anchored by two emojis, one happy and the other unhappy. The scale ranged from to 10, with replaced by the happy emoji. Trials were jittered by an inter-trial interval selected from a 2-5 s range, during which a black fixation

cross on a grey screen was presented (Figure 4B). DAs played one block where the decision target was the PR; and another where it was themselves. Block order was randomized across participants, as were buttons assigned to gambles or choices (left and right, to avoid lateralization effects) and placement of happy/unhappy emojis (left/right). Pain was genuinely administered to the DA during DA target blocks, but no actual pain was delivered during PR-target blocks.

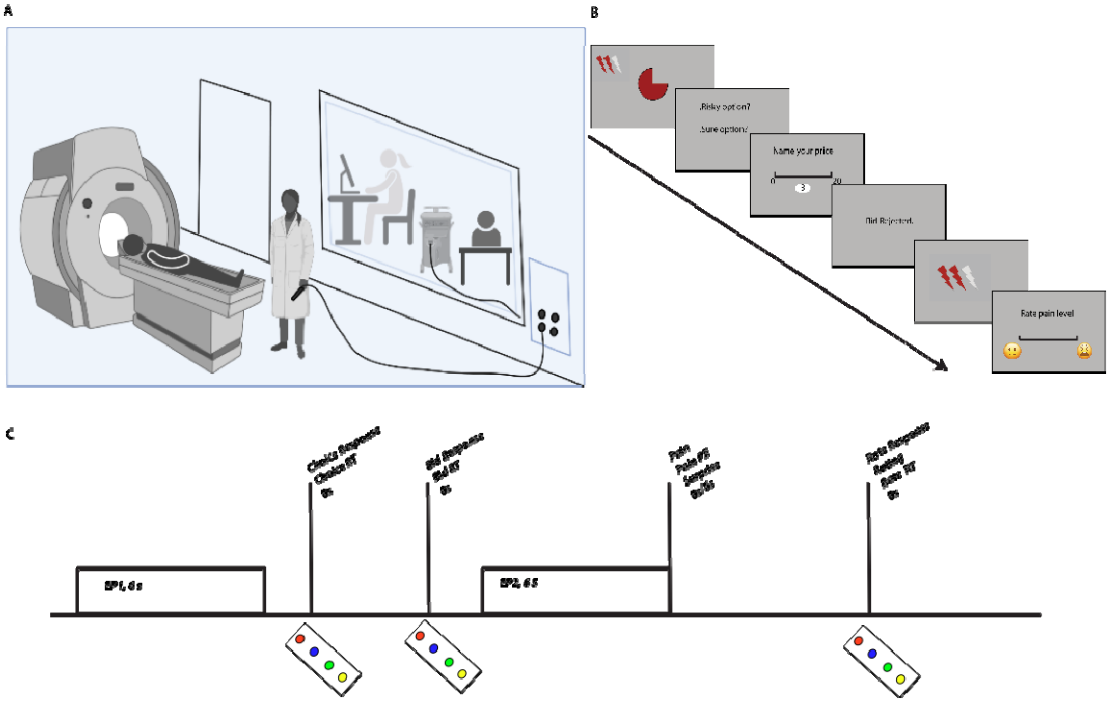

Figure 2 *A) Experimental setup. Deciding agents made decisions on threatened pain for themselves and others during an fMRI session. An experimenter delivered pain via laser within the scanner room. The participant was made to believe the other remained in the control room and was subject to pain delivery during the "Other" block condition. B) Sample Trial. Participants were first shown a visual cue representing an initial value of expected pain with the probability of delivery exhibited in a pie chart, and pain intensity by red lightning bolts. They were then asked to 1) either gamble to avoid pain or; 2) choose a sure option to reduce pain. They were then asked to place a monetary bid on their choice, which was then compared to a hidden, randomly generated reserve price. The participant was then told whether the bid was accepted or not, and the pain outcome was subsequently shown or delivered based on the expected value of the threatened pain following bid outcome. Participants were then asked to rate the perceived pain, for themselves in the "Self" condition, or the other felt in the related condition. C) fMRI Design. The general linear model constructed for fMRI analysis included, 1) cue onsets, parametric modulated for expected value and risk; 2) Choice onsets, modulated by choice response time; Bid onsets, modulated by bid RT; 3) Bid outcome modulated by expected value and risk; 4) Pain outcome, modulated by pain intensity, signed pain prediction error and surprise; 5) Rating onset, modulated by rating response time.*

Prior to performing the tasks, DAs played 3 practice rounds of the task, with the experimenter guiding them through each screen over the microphone. Only once participants confirmed their understanding of the task did the latter commence. Further, each block began with task instructions presented onscreen. Participants could begin the task when ready, by pressing a button. At the end of the two experimental runs, one payout of the blocks was randomly selected as payment (rounded down or up to the nearest integer) in addition to time paid for participating (50 CHF). Finally, we acquired the T1-MPRAGE anatomical scan, before removing the DA from the scanner. Once out of the scanner, the DA filled out a short series of questionnaires, before being paid, debriefed and sent home.

Computational Models

To capture the underlying inference hypothesized in this paper, we apply computational models of decision-making under uncertainty to characterize neural processes related to presented stimuli and outcome; and to explain observed behavioral choices. We employ pre-existing models testing the effect of uncertainty on economic decision-making[57], adapted to the domain of pain assessment and treatment.

Computational Model Equations

We employed computational models to quantify key variables related to decision-making under pain uncertainty. These variables were calculated on a trial-by-trial basis.

Expected Pain at Cue Presentation (EP_1) At the initial cue presentation, the expected pain (EP_1) represents the average pain intensity given the probabilities of the outcomes. Assuming one outcome is a potential pain intensity P, with probability p_1, and the other outcome is no pain (intensity):

$$EP_1 = p_1 \cdot P + (1 - p_1) \cdot 0$$

$$EP_1 = p_1 \cdot P$$

Where:

- P: The threatened pain stimulation intensity (e.g., 2 or 3 lightning bolts).
- p_1: The initial probability of experiencing pain P (from the visual pie chart).

Initial Risk (σ_1^2) Initial risk (σ_1^2) quantifies the uncertainty (variance) associated with the expected pain at cue presentation. Given the same two outcomes (P with probability p_1, and with probability $1-p_1$), the variance is calculated as:

$$\sigma_1^2 = p_1 \cdot P^2 - (EP_1)^2$$

This simplifies to:

$$\sigma_1^2 = p_1 \cdot P^2 - (p1 \cdot P)^2$$
$$\sigma_1^2 = p_1 \cdot P^2 - p12 \cdot P^2$$
$$\sigma_1^2 = p_1 \cdot P^2 (1-p_1)$$

Expected Pain After Bid Outcome (EP_2) Following the bid outcome, the expected pain (EP_2) is updated based on the participant's choice (gamble or sure option) and whether the bid was accepted.

If the gamble option was chosen and the bid was accepted: The probability of pain is halved (to $p_1/2$), and the other outcome remains .

$$EP_2 = p_1/2 \cdot P + (1 - p_1/2) \cdot$$

$$EP_2 = p_1/2 \cdot P$$

If the sure option was chosen and the bid was accepted: The pain intensity is reduced by one level ($P - 1$), and the probability of this reduced pain remains p_1. The other outcome remains .

$$EP_2 = p_1 \cdot (P-1) + (1-p_1) \cdot$$

$$EP_2 = p_1 \cdot (P-1)$$

If the bid was rejected (for either gamble or sure choice): The expected pain remains the initial EP_1.

$$EP_2 = EP_1$$

Risk After Bid Outcome (σ_2^2) Risk (σ_2^2) is updated similarly based on the bid outcome and choice.

If the gamble option was chosen and the bid was accepted: The variance is calculated with the new probability $p_1/2$ and pain intensity P.

$$\sigma_2^2 = p_1/2 \cdot P^2(1 - p_1/2)$$

If the sure option was chosen and the bid was accepted: The variance is calculated with the original probability p_1 and the reduced pain intensity ($P-1$).

$$\sigma_2^2 = p_1 \cdot (P-1)^2 (1-p_1)$$

If the bid was rejected (for either gamble or sure choice): The risk remains the initial σ_1^2.

$$\sigma_2^2 = \sigma_1^2$$

Pain Outcome (P_o) P_o is the actual pain experienced or witnessed at the trial outcome.

Signed Pain Prediction Error (δ_{pain}) Following the delivery of pain, the signed pain prediction error (δ_{pain}) is the difference between the observed pain outcome and the updated expected pain:

$$\delta_{pain} = P_o - EP_2$$

Risk Prediction used as "Surprise" : The risk prediction error, referred to as "Surprise" throughout the study, quantifies the deviation of the squared signed prediction error from the expected variance after the bid outcome. This is an unsigned error, reflecting the unexpectedness of the outcome's magnitude relative to the updated uncertainty[57].

$$Surprise = (\delta_{pain})^2 - \sigma_2^2$$

Subjective Probability Weighting (Bid Model)

To assess whether participants distorted objective pain probabilities during decision-making, we fitted a one-parameter Prelec probability weighting function [55]to each participant's bids, separately for self and other conditions. The Prelec function transforms objective probabilities *p* into subjective decision weights:

$$w(p) = exp(-(-ln\ p)^\alpha)$$

where $\alpha = 1$ indicates no distortion (objective model), $\alpha < 1$ indicates overweighting of small probabilities (inverse-S shaped distortion), and $\alpha > 1$ indicates overweighting of large probabilities. Using each participant's fitted α, we computed subjective expected pain ($sEP = w(p) \times Pain$) and subjective risk ($sRisk = w(p) \times Pain^2 \times (1 - w(p))$), as well as subjective prediction error and surprise derived from these quantities.

The bid model assumed that participants' bids were a linear function of subjective expected pain and subjective risk:

$$Bid = \beta_0 + \beta_1 \times sEP + \beta_2 \times sRisk + \varepsilon$$

where $\varepsilon \sim N(0, \sigma^2)$. Five parameters ($\alpha$, β_0, β_1, β_2, σ) were estimated per participant per target condition by minimizing the negative log-likelihood using unconstrained Nelder-Mead optimization (MATLAB fminsearch) with 20 random restarts. Parameter bounds were enforced via sigmoid ($\alpha \in [0.1, 3.0]$) and exponential ($\sigma >$) transforms. A null model fixing $\alpha = 1$ (no probability distortion) was fitted for comparison. Model comparison was performed using AIC.

Two participants (subjects 12 and 22) who placed zero bids on all self-condition trials were excluded from self-condition model fitting (α set to 1.0 for fMRI regressor computation). All other 64 subject-condition fits converged successfully.

Data Analysis

Behavioral

Behavioral data analyisis was performed using Matlab 2014b. We analyzed overt, behavioral responses as a function of decision-making variables listed above; and decision targets. We first modelled participants behavioral responses at the level of 1) choice; 2) bids and 3) ratings. We constructed a linear mixed model under the binomial distribution, casting choice (0 = gamble, 1 = sure option) as a function of EP_1, $Risk_1$, and choice reaction time (RT), as well as their interactions with the target (Self or Other). In the second, we constructed a general linear model casting bids as a function of EP_1, $Risk_1$, choice, and bid RT, as well as their interactions with the target. In the third, we constructed a general linear model casting pain rating as a function of pain, pain prediction error, pain surprise, and rating RT, as well as their interactions with the target. In all models, gender was specified as a nuisance fixed

factor, and partipants' identifier as a random factor (see Table 5). These models can capture how covert computations relating to uncertainty (expected pain values, pain risk, pain prediction error and pain surprise) may affect overt behavior, and distinguish potential differences in their effects on the target (Table 5).

Table 5: Description of Generalized Linear Models for Behavioral Responses This table outlines the structure of the three generalized linear mixed-effects (GLME) models used to analyze participants' behavioral responses. Each model specifies the outcome variable, primary predictor variables, nuisance variables (fixed factors), and random effects (participant-level intercepts).

Model	Outcome Variable	Predictor Variables	Nuisance Variables	Random Effects
Model 1 (binomial)	Choice	EP_1, $Risk_1$, Target,	Sex	Participant
Model 2	Bid	EP_1, $Risk_1$, bid RT, choice, Target	Sex	Participant
Model 3	Rating	Pain, Pain PE, Pain Surprise, choice, bids, rate RT, Target	Sex	Participant

Neuroimaging analysis

Neuroimaging preprocessing and analysis was performed using SPM12. The main goal of the neuroimaging analysis was to apply a model-based approach to BOLD responses at specific timepoints of the trial that do not require an overt response from the participant. We first describe the preprocessing pipeline applied to the functional MR datasets below.

Preprocessing

Functional MR volumes were first converted to nifti format from dicom. Images were then slice-time corrected to the middle slice (36). Voxel displacement maps were then applied to the images, before the latter were realigned and unwarped according to head motion parameters (6; 3 translational and 3 rotational). Individual T1w anatomical volumes were then co-registered to the mean functional images and segmented according to six-class tissue probability maps (TPMs). The resulting parameters (forward deformations) were then applied to functional volumes, which were then normalized to the standard MNI152 template, before being smoothed to a FWHM of 8 mm. The resulting preprocessed images were used for analysis.

Univariate analysis - Voxelwise

In a first instance, we constructed a general linear model including the following onsets: cue presentation (0s); choice response (0s); bid response (0s); bid outcome (0s); trial outcome (0s for self, and 6s for other, respectively); and rating response (0s). These onsets were convolved with the canonical hemodynamic response function and parametrically modulated by the expected value and risk following choice; choice RT; the expected value and risk following bids; bid RT; pain level, pain prediction error (signed PE) and pain surprise (unsigned PE) following trial outcome; and rating and rating RT following pain evaluation. All parametric modulators were serially orthogonalized relative to one another. In addition, we included 24 noise regressors comprised of the 6 motion parameters and 18 cardiac and respiratory regressors (TAPAS toolbox). We employed the FAST algorithm to control for auto-correlation. The general linear model was performed on individual subject timeseries first, before pooling resulting contrasts of interest in a second-level, random-effects model to test group-level responses. Group analyses effects were considered significant if exceeding a threshold corresponding to $p < .05$ FWE corrected for multiple comparisons at the cluster level, with an underlying voxel-based threshold corresponding to $p < 1$ (uncorrected)[18].

Contrasts of interest focused on the following elements of the computational model, split into predictive and trial outcome phases. In the predictive phase, we tested for expected value of pain and pain risk (concatenating regressors from onsets at cue presentation and following bid outcome). In the trial outcome phase, we tested for pain intensity, signed prediction error and pain surprise (unsigned prediction error).

Group-level random-effects analyses were performed using one-sample t-tests on first-level contrast images. Two thresholds were applied: (1) whole-brain voxel-level FWE correction at $p < .05$; (2) a voxel-level threshold of $p < 5$ (uncorrected) with cluster-level FWE correction at $p < .05$ (minimum cluster extent $k = 25$ voxels).

Univariate analysis – Region-based

To complement the mass univariate approach at the whole brain level, we selected 4 brain regions involved in inferential processes: the anterior insula; the anterior cingulate; caudate and putamen (dorsal striatum). In addition, for surprise contrasts, we used ROIs centered on previously published peak BOLD responses for surprise in perceptual and valued-based decision-making[41]. Region-of-interest analyses were performed using small volume

correction within anatomically defined bilateral masks of the anterior insula, anterior cingulate cortex, caudate nucleus, and putamen. An initial voxel-level threshold of $p < 5$ (uncorrected) was applied, followed by FWE correction at $p < .05$ within each small volume.

Beta extraction

For each participant, mean parameter estimates were extracted from first-level contrast images within each ROI. Group-level significance was assessed via one-sample t-tests (testing whether mean beta differed from zero) and paired t-tests (comparing self vs. other conditions within each ROI).

Multivariate Neuroimaging Analysis

To perform the following multivariate analyses, we first derived single-trial beta estimates using a Least-Squares Separate (LSS) approach. Given the distinct temporal phases of the task, two separate GLMs were constructed to optimize signal estimation. For variables related to the predictive phase (Expected Pain and Risk), betas were estimated at cue onset using an LSS model where each cue trial was modeled as an individual regressor, while outcome events were collapsed into a single regressor. Conversely, for variables related to the post-outcome phase (Signed Prediction Error and Surprise), trial-wise betas were estimated at the point of pain delivery using an LSS model where each outcome event was modeled individually and cue events were collapsed. This dual-model approach ensured that single-trial estimates for predictive vs. outcome-related signals were maximized for sensitivity while minimizing spillover between trial phases.

Respresentational Similarity Analysis

Within-subject RSA was performed using the phase-appropriate single-trial beta series described above. For each participant and target condition (self, other), trial-wise voxel patterns were extracted within each ROI. Neural representational dissimilarity matrices (RDMs) were computed as 1 minus the Pearson correlation between these patterns. Model RDMs were constructed from the absolute pairwise differences of trial-wise computational variables (EP, Risk, Signed PE, and Surprise). The correspondence between neural and model RDMs was quantified using Spearman rank correlation. Statistical significance of individual-subject RSA values was assessed via permutation testing (5,000 permutations). Group-level inference used one-sample t-tests on Fisher-z-transformed correlations, with paired t-tests comparing self and other conditions.

Encoding model

As a complementary multivariate approach, we computed voxelwise encoding scores within each ROI. For each participant, target condition, and voxel, we computed the Pearson correlation between the trial-wise LSS beta series and the computational variable of interest. Voxelwise correlations were Fisher-z-transformed and averaged across voxels within each ROI, yielding one encoding score per participant per condition per ROI. Group statistics were performed using one-sample and paired t-tests on these encoding scores.

Acknowledgments: This study is funded by the Swiss National Science Foundation grant PP00P1_183715 awarded to CCD. Neuroimaging data can be found here: https://osf.io/da7tw/overview; related behavioral data here: https://osf.io/uqtcw/overview and related code, here: https://github.com/LLouedKhen/OPPI_Project_Unige2021.

Conflict of Interest Statement: The authors declare no conflicts of interest related to this work.

References

[1] Andreoni J, Rao JM, Trachtman H. Avoiding the Ask: A Field Experiment on Altruism, Empathy, and Charitable Giving. Journal of Political Economy 2017;125:625–653.

[2] Asakura N, Inui T. A Bayesian Framework for False Belief Reasoning in Children: A Rational Integration of Theory-Theory and Simulation Theory. Front Psychol 2016;7. doi:10.3389/fpsyg.2016.02019.

[3] Atlas LY, Wager TD. How expectations shape pain. Neuroscience Letters 2012;520:140–148.

[4] Bach DR, Dolan RJ. Knowing how much you don't know: a neural organization of uncertainty estimates. Nature Reviews Neuroscience 2012;13:572–586.

[5] Barnby JM, Raihani N, Dayan P. The self as a prior for the other: social learning under paranoia. 2021. doi:10.31234/osf.io/an5kp.

[6] Batson CD. Altruism in Humans. Oxford University Press, 2010.

[7] Benuzzi F, Lui F, Ardizzi M, Ambrosecchia M, Ballotta D, Righi S, Pagnoni G, Gallese V, Porro CA. Pain Mirrors: Neural Correlates of Observing Self or Others' Facial Expressions of Pain. Front Psychol 2018;9. doi:10.3389/fpsyg.2018.01825.

[8] Birmingham E, Bischof WF, Kingstone A. Social Attention and Real-World Scenes: The Roles of Action, Competition and Social Content. Quarterly Journal of Experimental Psychology 2008;61:986–998.

[9] Bonnet C, Fauquet Ars J, Estaún Ferrer S. Reaction times as a measure of uncertainty. Psicothema 2008;20:43–48.

[10] Boring BL, Ng BW, Nanavaty N, Mathur VA. Over-Rating Pain is Overrated: A Fundamental Self-Other Bias in Pain Reporting Behavior. The Journal of Pain 2022;23:1779–1789.

[11] Brown CA, Seymour B, Boyle Y, El-Deredy W, Jones AKP. Modulation of pain ratings by expectation and uncertainty: Behavioral characteristics and anticipatory neural correlates. PAIN 2008;135:240–250.

[12] Büchel C. The role of expectations, control and reward in the development of pain persistence based on a unified model. eLife 2023;12:e81795.

[13] Büchel C, Geuter S, Sprenger C, Eippert F. Placebo Analgesia: A Predictive Coding Perspective. Neuron 2014;81:1223–1239.

[14] Clark A. Whatever next? Predictive brains, situated agents, and the future of cognitive science. Behavioral and Brain Sciences 2013;36:181–204.

[15] Clark JA, Brown CA, Jones AKP, El-Deredy W. Dissociating nociceptive modulation by the duration of pain anticipation from unpredictability in the timing of pain. Clinical Neurophysiology 2008;119:2870–2878.

[16] Corradi-Dell'Acqua C, Tusche A, Vuilleumier P, Singer T. Cross-modal representations of first-hand and vicarious pain, disgust and fairness in insular and cingulate cortex. Nat Commun 2016;7:1–12.

[17] Dirupo G, Totaro S, Richard J, Corradi-Dell'Acqua C. Medical education and distrust modulate the response of insular-cingulate network and ventral striatum in pain diagnosis. Elife 2021;10:e63272.

[18] Eklund A, Nichols T, Knutsson H. Can parametric statistical methods be trusted for fMRI based group studies? Proc Natl Acad Sci USA 2016;113:7900–7905.

[19] Fazeli S, Büchel C. Pain-Related Expectation and Prediction Error Signals in the Anterior Insula Are Not Related to Aversiveness. J Neurosci 2018;38:6461–6474.

[20] Fehr E, Rockenbach B. Human altruism: economic, neural, and evolutionary perspectives. Current Opinion in Neurobiology 2004;14:784–790.

[21] Fields HL. How expectations influence pain. PAIN 2018;159:S3.

[22] Gallese V. Before and below 'theory of mind': embodied simulation and the neural correlates of social cognition. Philosophical Transactions of the Royal Society B: Biological Sciences 2007;362:659–669.

[23] Geuter S, Boll S, Eippert F, Büchel C. Functional dissociation of stimulus intensity encoding and predictive coding of pain in the insula. eLife 2017;6:e24770.

[24] Hoskin R, Berzuini C, Acosta-Kane D, El-Deredy W, Guo H, Talmi D. Sensitivity to pain expectations: A Bayesian model of individual differences. Cognition 2019;182:127–139.

[25] Hoskin R, Talmi D. Adaptive coding of pain prediction error in the anterior insula. European Journal of Pain 2023;27:766–778.

[26] Hutcherson CA, Bushong B, Rangel A. A Neurocomputational Model of Altruistic Choice and Its Implications. Neuron 2015;87:451–462.

[27] Isnard J, Magnin M, Jung J, Mauguière F, Garcia-Larrea L. Does the insula tell our brain that we are in pain? PAIN® 2011;152:946–951.

[28] Jones CL, Minati L, Harrison NA, Ward J, Critchley HD. Under pressure: Response urgency modulates striatal and insula activity during decision-making under risk. PLoS ONE 2011;6.

[29] Kahneman D, Tversky A. Prospect Theory: An Analysis of Decision under Risk. Econometrica 1979;47:263–291.

[30] Kappesser J, Williams AC de C, Prkachin KM. Testing two accounts of pain underestimation. Pain 2006;124:109–116.

[31] Knill DC, Pouget A. The Bayesian brain: The role of uncertainty in neural coding and computation. Trends in Neurosciences 2004;27:712–719.

[32] Knutson B, Huettel SA. The risk matrix. Current Opinion in Behavioral Sciences 2015;5:141–146.

[33] Korucuoglu O, Harms MP, Astafiev SV, Kennedy JT, Golosheykin S, Barch DM, Anokhin AP. Test-retest reliability of fMRI-measured brain activity during decision making under risk. NeuroImage 2020;214:116759.

[34] Krishnan A, Woo C-W, Chang LJ, Ruzic L, Gu X, López-Solà M, Jackson PL, Pujol J, Fan J, Wager TD. Somatic and vicarious pain are represented by dissociable multivariate brain patterns. eLife 2016;5:e15166.

[35] Lamm C, Decety J, Singer T. Meta-analytic evidence for common and distinct neural networks associated with directly experienced pain and empathy for pain. NeuroImage 2011;54:2492–2502.

[36] Lang S, Yu T, Markl A, Müller F, Kotchoubey B. Hearing others' pain: neural activity related to empathy. Cogn Affect Behav Neurosci 2011;11:386–395.

[37] Lockwood PL, Wittmann MK, Apps MAJ, Klein-Flügge MC, Crockett MJ, Humphreys GW, Rushworth MFS. Neural mechanisms for learning self and other ownership. Nature Communications 2018;9:1–11.

[38] Loued-Khenissi L, Corradi-Dell'Acqua C. Gambling on others' health: risky pro-social decision-making in the era of COVID-19. Front Psychol 2024;15. doi:10.3389/fpsyg.2024.1370778.

[39] Loued-Khenissi L, Martin-Brevet S, Schumacher L, Corradi-Dell'Acqua C. The effect of uncertainty on pain decisions for self and others. European Journal of Pain 2022;26:1163–1175.

[40] Loued-Khenissi L, Martin-Brevet S, Schumacher L, Corradi-Dell'Acqua C. The effect of uncertainty on pain decisions for self and others. European Journal of Pain 2022;26:1163–1175.

[41] Loued-Khenissi L, Pfeuffer A, Einhäuser W, Preuschoff K. Anterior insula reflects surprise in value-based decision-making and perception. NeuroImage 2020:116549.

[42] Lutz A, McFarlin DR, Perlman DM, Salomons TV, Davidson RJ. Altered anterior insula activation during anticipation and experience of painful stimuli in expert meditators. NeuroImage 2013;64:538–46.

[43] Markowitz HM. Portfolio selection. Journal of Finance 1952;7:77–91.

[44] McGovern HT, Otten M. Priors and prejudice: hierarchical predictive processing in intergroup perception. Front Psychol 2024;15. doi:10.3389/fpsyg.2024.1386370.

[45] Mishra S. Decision-Making Under Risk: Integrating Perspectives From Biology, Economics, and Psychology. Pers Soc Psychol Rev 2014;18:280–307.

[46] Moayedi M. All roads lead to the insula. PAIN 2014;155:1920.

[47] Mohr PNC, Biele G, Heekeren HR. Neural processing of risk. The Journal of neuroscience : the official journal of the Society for Neuroscience 2010;30:6613–9.

[48] O'Doherty JP, Hampton A, Kim H. Model-based fMRI and its application to reward learning and decision making. Ann N Y Acad Sci 2007;1104:35–53.

[49] Palermo S, Benedetti F, Costa T, Amanzio M. Pain anticipation: An activation likelihood estimation meta-analysis of brain imaging studies. Human Brain Mapping 2015;36:1648–1661.

[50] Peerdeman KJ, van Laarhoven AIM, Keij SM, Vase L, Rovers MM, Peters ML, Evers AWM. Relieving patients' pain with expectation interventions: a meta-analysis. PAIN 2016;157:1179.

[51] Pereda M, Brañas-Garza P, Rodríguez-Lara I, Sánchez A. The emergence of altruism as a social norm. Sci Rep 2017;7:9684.

[52] Peter E, Watt-Watson J. Unrelieved Pain: An Ethical and Epistemological Analysis of Distrust in Patients. Canadian Journal of Nursing Research Archive 2002. Available: https://cjnr.archive.mcgill.ca/article/view/1765. Accessed 12 Feb 2025.

[53] Ploghaus A, Becerra L, Borras C, Borsook D. Neural circuitry underlying pain modulation: expectation, hypnosis, placebo. Trends in Cognitive Sciences 2003;7:197–200.

[54] Polman E, Wu K. Decision making for others involving risk: A review and meta-analysis. Journal of Economic Psychology 2020;77:102184.

[55] Prelec D. The Probability Weighting Function. Econometrica 1998;66:497–527.

[56] Preuschoff K, Bossaerts P, Quartz SR. Neural Differentiation of Expected Reward and Risk in Human Subcortical Structures. Neuron 2006;51:381–390.

[57] Preuschoff K, ’t Hart BM, Einhäuser W. Pupil Dilation Signals Surprise: Evidence for Noradrenaline’s Role in Decision Making. Frontiers in neuroscience 2011;5:115.

[58] Preuschoff K, Quartz SR, Bossaerts P. Human insula activation reflects risk prediction errors as well as risk. The Journal of neuroscience : the official journal of the Society for Neuroscience 2008;28:2745–52.

[59] Prkachin KM, Solomon PE, Ross J. Underestimation of Pain by Health-Care Providers: Towards a Model of the Process of Inferring Pain in Others. Canadian Journal of Nursing Research Archive 2007:88–106.

[60] R G, C S, S B, Ag M, Td W, M R. Neurophysiological encoding of aversive prediction errors. Pain 2025. doi:10.1097/j.pain.0000000000003712.

[61] Seers T, Derry S, Seers K, Moore RA. Professionals underestimate patients’ pain: a comprehensive review. Pain 2018;159:811–818.

[62] Sharvit G, Corradi-Dell Acqua C, Vuilleumier P. Modality-specific effects of aversive expectancy in the anterior insula and medial prefrontal cortex. Pain 2018;159:1529–1542.

[63] Sharvit G, Vuilleumier P, Corradi-Dell’Acqua C. Sensory-specific predictive models in the human anterior insula. 2019. doi:10.12688/f1000research.17961.1.

[64] Siman-Tov T, Granot RY, Shany O, Singer N, Hendler T, Gordon CR. Is there a prediction network? Meta-analytic evidence for a cortical-subcortical network likely subserving prediction. Neurosci Biobehav Rev 2019;105:262–275.

[65] Song Y, Kemprecos H, Wang J, Chen Z. A Predictive Coding Model for Evoked and Spontaneous Pain Perception. 2019 41st Annual International Conference of the IEEE Engineering in Medicine and Biology Society (EMBC).2019. pp. 2964–2967.

[66] Stone ER, YoonSun C, Bruine de Bruin W, Mandel DR. I can take the risk, but you should be safe: Self-other differences in situations involving physical safety. Judgment and Decision Making 2013;8:250–267.

[67] Summerfield C, Lange FPD. Expectation in perceptual decision making : neural and computational mechanisms. Nature Publishing Group 2014. doi:10.1038/nrn3838.

[68] Sun C, Qian H, Miao C. From Psychological Curiosity to Artificial Curiosity: Curiosity-Driven Learning in Artificial Intelligence Tasks. 2022. doi:10.48550/arXiv.2201.08300.

[69] Tabor A, Burr C. Bayesian Learning Models of Pain: A Call to Action. Curr Opin Behav Sci 2019;26:54–61.

[70] Tobler PN, O'Doherty JP, Dolan RJ, Schultz W. Reward Value Coding Distinct From Risk Attitude-Related Uncertainty Coding in Human Reward Systems. Journal of Neurophysiology 2006;97:1621–1632.

[71] Tom SM, Fox CR, Trepel C, Poldrack R a. The neural basis of loss aversion in decision-making under risk. Science (New York, NY) 2007;315:515–8.

[72] Tracey I, Mantyh PW. The Cerebral Signature for Pain Perception and Its Modulation. Neuron 2007;55:377–391.

[73] Trepel C, Fox CR, Poldrack RA. Prospect theory on the brain? Toward a cognitive neuroscience of decision under risk. Cognitive Brain Research 2005;23:34–50.

[74] Treue S. Visual attention: the where, what, how and why of saliency. Current Opinion in Neurobiology 2003;13:428–432.

[75] Wiech K. Deconstructing the sensation of pain: The influence of cognitive processes on pain perception. Science 2016;354:584–587.

[76] Yoshida W, Seymour B, Koltzenburg M, Dolan RJ. Uncertainty Increases Pain: Evidence for a Novel Mechanism of Pain Modulation Involving the Periaqueductal Gray. J Neurosci 2013;33:5638–5646.

[77] Zaki J, Wager TD, Singer T, Keysers C, Gazzola V. The Anatomy of Suffering: Understanding the Relationship between Nociceptive and Empathic Pain. Trends in Cognitive Sciences 2016;20:249–259.

[78] Zaman J, Van Oudenhove L, Vlaeyen JWS. Uncertainty in a context of pain: disliked but also more painful? PAIN 2021;162:995–998.

Supplementary Materials

S1. Full univariate results

Table S1.1 Small volume correction results. Significant (p(FWE) < .05, marked *) and marginal (p(FWE) < 0.010, marked ~) peaks within ROIs. Initial threshold p < 0.005 uncorrected. Anterior insula surprise spheres from Loued-Khenissi et al. (2020)

Contrast	ROI	x	y	z	Peak T	p(FWE)	k	
Risk, Self	L Caudate	−16	18	12	3.97	0.017	29	*
Risk, Other	L Putamen	−22	2	8	5.28	<0.001	396	*
	R Putamen	28	−6	−4	5.37	<0.001	306	*
	L Caudate	−14	2	18	4.58	0.004	193	*
	R Caudate	18	2	16	4.69	0.003	128	*
	L Anterior Insula	−44	4	−6	3.96	0.025	75	*
	R Anterior Insula	36	6	4	3.86	0.031	77	*
	L AIns surp. sphere□	−28	10	−2	3.26	0.066	36	~
	R AIns surp. sphere□	46	28	−14	3.07	0.095	7	~
Surprise, Self	R AIns surp. sphere□	48	26	−10	3.90	0.016	91	*
	L Anterior Insula	−38	16	−14	3.42	0.077	6	~
	R Caudate	12	−2	18	3.35	0.068	19	~
Surprise, Other	R AIns surp. sphere□	44	26	−2	3.43	0.039	39	*

□ *Loued-Khenissi et al. (2020) anterior insula surprise sphere.* □

Table S1.2 ROI beta extraction results. One-sample t-tests (H□: β =) and paired self-vs-other comparisons. Only significant results shown (p < .05). *** p < 0.001; ** p < .01; * p < .05.

Contrast	ROI	Mean β	SE	t(32)	p	
EP, Self	L ACC	−0.358	0.121	−2.95	0.006	**
	R ACC	−0.364	0.139	−2.61	0.014	*
Risk, Other	L Anterior Insula	0.367	0.114	3.21	0.003	**
	R Anterior Insula	0.305	0.132	2.32	0.027	*
	L Caudate	0.478	0.161	2.96	0.006	**
	R Caudate	0.358	0.145	2.47	0.019	*
	L Putamen	0.531	0.142	3.73	<0.001	***
	R Putamen	0.421	0.123	3.42	0.002	**
PE, Self	L Caudate	0.637	0.300	2.12	0.041	*
Surp, Self	R AIns surp. sphere	0.371	0.168	2.21	0.035	*
Surp, Other	R AIns surp. sphere	0.150	0.073	2.06	0.047	*
Self vs Other	**ROI**	**Diff**	**SE**	**t(32)**	**p**	

EP S < O	L ACC	−0.347	0.167	−2.08	0.046	*
	L Caudate	−0.411	0.175	−2.34	0.026	*
Risk S < O	R Anterior Insula	−0.533	0.226	−2.36	0.025	*
	L Putamen	−0.523	0.243	−2.15	0.039	*
	R Putamen	−0.493	0.225	−2.19	0.036	*
	R AIns surp. sphere	−0.582	0.262	−2.22	0.033	*
PE S > O	L Caudate	0.705	0.318	2.22	0.034	*

S2. Prelec probability weighting model

Prelec probability weighting functions were successfully fitted to 64 of 66 subject-condition combinations (31 self, 33 other). Median α values were .818 (self) and .971 (other), indicating modest probability distortion centered near the identity function. The subjective model did not reliably outperform the objective model: the subjective model was favored by AIC in only 9 of 31 self and 12 of 33 other participant fits. Weighting parameters did not differ between pain targets (Wilcoxon signed-rank p = .40). Objective and subjective regressors were highly correlated (EP: median r = .98; Risk: median r = .86), supporting the use of objective task-derived regressors as parametric modulators in the fMRI analysis. The following results are reported using the objective regressors; a supplementary analysis confirmed convergence with subjective regressors for all key findings.

Table S2.1 reports the fitted Prelec α parameters for each condition. Figure S1 shows individual probability weighting curves overlaid with the group mean, separately for self and other.

Table S2.1 *Prelec α parameter estimates from the bid model.*

	n fitted	Median α	Mean α	Min	Max	AIC wins
Self	31	0.818	1.135	0.100	3	9/31
Other	33	0.971	1.456	0.100	3	12/33

The Wilcoxon signed-rank test comparing α values between self and other conditions was not significant (p = .42, n = 31 paired), indicating that probability distortion did not differ by target condition.

S3. Objective vs. subjective regressor correlations

Table S3.1 *Per-subject correlations between objective and subjective regressors.*

Regressor	Target	Median r	Min r	Max r	MAD	n

EP	Self	0.9775	0.7018	1 0	0.2816	33
EP	Other	0.9624	0.7018	1 0	0.3390	33
Risk	Self	0.8640	0.7458	1 0	0.3071	33
Risk	Other	0.8061	0.7458	0.9997	0.4052	33

Expected pain regressors were highly correlated between objective and subjective formulations (median $r > .96$), while risk regressors diverged more substantially (median r = .81–0.86), reflecting the nonlinear dependence of variance on the probability weighting function.

S4. Choice model

A choice-level model was additionally fitted, estimating three parameters per participant per condition: α (Prelec curvature), β (inverse temperature), and θ (risk attitude, where positive values indicate risk aversion). Of 66 participant-condition pairs, 58 had sufficient choice variability for fitting. However, the inverse temperature parameter β converged to near zero for approximately half of participants, rendering the risk attitude parameter θ unidentifiable (values ranged from -53×10^6 to $+3.5 \times 10^6$). This reflects the fundamental limitation of fitting three free parameters to 18 binary observations. Among the subset of participants with interpretable fits ($\beta > .5$; approximately 15 participants), θ values clustered in the range .2–1.7, qualitatively consistent with the risk aversion observed in the behavioral GLMEs, but the reduced sample precluded reliable self vs. other comparison. The choice model was therefore not used for neuroimaging regressors.

S5. Whole-brain results with subjective regressors

Full univariate results using Prelec-model derived subjective regressors (see S1)

Contrast	Threshold	Region	X	Y	Z	peak_T	peak_pFWE	k_voxels	cluster_pFWE
EP_S	unc005_k25	Right SOG superior occipital gyrus	28	-92	18	4.156	0.920	215	0
EP_S	unc005_k25	Left SFG superior frontal gyrus	-22	4	62	3.726	0.998	151	0
EP_S	unc005_k25	Left SPL superior parietal lobule	-10	-64	64	3.118	1.000	42	0
EP_O	FWE_p05	Right SOG superior occipital gyrus	28	-90	16	7.703	0.001	109	0
EP_O	FWE_p05	Left Cerebral White Matter	-22	-92	16	5.893	0.047	2	<0.001
EP_O	unc005_k25	Right SOG superior occipital gyrus	28	-90	16	7.703	0.001	2653	0

EP_O	unc005_k25	Left Cerebral White Matter	-22	-92	16	5.893	0.047	2611	0
EP_O	unc005_k25	Left SMC supplementary motor cortex	-4	16	42	4.745	0.519	1444	0
EP_O	unc005_k25	Unknown	14	-76	58	3.208	1.000	119	0
EP_O	unc005_k25	Left Cerebellum White Matter	-26	-46	-46	3.704	0.999	110	0
EP_O	unc005_k25	Left Cerebral White Matter	-6	-38	30	3.986	0.979	91	0
EP_O	unc005_k25	Left FO frontal operculum	-46	8	-2	3.300	1.000	77	0
EP_O	unc005_k25	Right Lateral Ventricle	32	-38	-2	3.681	0.999	61	0
EP_O	unc005_k25	Right PrG precentral gyrus	26	-12	52	3.623	1.000	57	0
EP_O	unc005_k25	Left PrG precentral gyrus	-18	-20	76	3.475	1.000	57	0
EP_O	unc005_k25	Unknown	2	-34	-2	4.159	0.932	39	0
EP_O	unc005_k25	Unknown	8	-44	-2	3.282	1.000	37	0
EP_O	unc005_k25	Left Cerebral White Matter	-50	-36	40	3.268	1.000	35	<0.001
EP_O	unc005_k25	Left PIns posterior insula	-36	4	-16	3.432	1.000	29	<0.001
EP_O	unc005_k25	Left AIns anterior insula	-32	10	8	3.280	1.000	29	<0.001
EP_O	unc005_k25	Left Cerebral White Matter	-28	-42	38	3.141	1.000	28	<0.001
EP_O	unc005_k25	Left Cerebral White Matter	-14	-42	8	3.097	1.000	27	<0.001
EP_O	unc005_k25	Left MFG middle frontal gyrus	-36	42	28	3.327	1.000	25	<0.001
Risk_S	unc005_k25	Left Ventral DC	-4	-10	-10	3.536	1.000	89	0
Risk_S	unc005_k25	Left Accumbens Area	-14	10	-12	3.986	0.966	85	0
Risk_S	unc005_k25	Right Lateral Ventricle	8	16	12	3.663	0.999	66	0
Risk_S	unc005_k25	Left Cerebral White Matter	-10	26	32	3.244	1.000	60	0
Risk_S	unc005_k25	Left Cerebral White Matter	-24	-32	42	4.912	0.352	60	0
Risk_S	unc005_k25	Left MFG middle frontal gyrus	-40	32	32	3.246	1.000	50	0

Risk_S	unc005_k25	Right Cerebral White Matter	20	34	22	3.280	1.000	48	0
Risk_S	unc005_k25	Right LiG lingual gyrus	10	-88	-10	3.436	1.000	39	0
Risk_S	unc005_k25	Right Lateral Ventricle	20	-38	14	3.252	1.000	35	<0.001
Risk_S	unc005_k25	Left Cerebral White Matter	-28	38	6	3.329	1.000	33	<0.001
Risk_S	unc005_k25	Left SMC supplementary motor cortex	-8	18	48	3.442	1.000	33	<0.001
Risk_S	unc005_k25	Left Lateral Ventricle	-24	-42	10	3.848	0.989	29	<0.001
Risk_S	unc005_k25	Left Cerebral White Matter	-20	-42	26	3.623	0.999	26	<0.001
Risk_O	unc005_k25	Right Calc calcarine cortex	16	-72	10	5.153	0.262	3731	NaN
Risk_O	unc005_k25	Left Cerebral White Matter	-28	16	6	4.762	0.529	2156	0
Risk_O	unc005_k25	Right TMP temporal pole	32	8	-28	4.182	0.935	632	0
Risk_O	unc005_k25	Cerebellar Vermal Lobules I-V	4	-54	-20	5.084	0.300	618	0
Risk_O	unc005_k25	Right Cerebral White Matter	16	8	8	3.868	0.995	225	0
Risk_O	unc005_k25	Unknown	32	12	64	4.429	0.797	219	0
Risk_O	unc005_k25	Right MFG middle frontal gyrus	30	0	52	4.179	0.936	184	0
Risk_O	unc005_k25	Right TrIFG triangular part of the inferior frontal gyrus	54	26	-2	3.968	0.986	178	0
Risk_O	unc005_k25	Left MCgG middle cingulate gyrus	-6	18	36	4.337	0.858	123	0
Risk_O	unc005_k25	Left TMP temporal pole	-46	8	-38	3.551	1.000	111	0
Risk_O	unc005_k25	Right Cerebellum Exterior	36	-48	-48	3.942	0.989	104	0
Risk_O	unc005_k25	Left ITG inferior temporal gyrus	-42	-18	-22	3.527	1.000	93	0
Risk_O	unc005_k25	Right Hippocampus	26	-30	-6	3.809	0.997	89	0
Risk_O	unc005_k25	Left SPL superior	-10	-70	54	3.425	1.000	89	0

		parietal lobule							
Risk_O	unc005_k25	Left Cerebellum Exterior	-22	-70	-22	4.318	0.869	88	0
Risk_O	unc005_k25	Left Cerebellum Exterior	-44	-66	-34	3.226	1.000	86	0
Risk_O	unc005_k25	Right Cerebral White Matter	50	-16	-32	3.370	1.000	86	0
Risk_O	unc005_k25	Left SMG supramarginal gyrus	-54	-42	30	3.377	1.000	77	0
Risk_O	unc005_k25	Left Cerebral White Matter	-24	-16	6	3.657	1.000	76	0
Risk_O	unc005_k25	Right SPL superior parietal lobule	20	-66	60	3.497	1.000	76	0
Risk_O	unc005_k25	Left Cun cuneus	-14	-78	26	3.465	1.000	71	0
Risk_O	unc005_k25	Right SMG supramarginal gyrus	60	-42	22	3.795	0.998	70	0
Risk_O	unc005_k25	Left SFG superior frontal gyrus	-22	-2	56	3.509	1.000	65	0
Risk_O	unc005_k25	Left Cerebral White Matter	-36	-70	28	3.465	1.000	64	0
Risk_O	unc005_k25	Right Thalamus Proper	12	-18	-2	4.679	0.597	60	0
Risk_O	unc005_k25	Left Cerebellum Exterior	-10	-62	-48	4.796	0.501	54	0
Risk_O	unc005_k25	Right TMP temporal pole	40	16	-42	3.315	1.000	51	0
Risk_O	unc005_k25	Right Cerebral White Matter	20	-18	58	4.426	0.799	42	0
Risk_O	unc005_k25	Right CO central operculum	50	6	0	3.528	1.000	40	0
Risk_O	unc005_k25	Left SMC supplementary motor cortex	-6	10	48	3.406	1.000	40	0
Risk_O	unc005_k25	Right Cerebral White Matter	38	-18	-4	3.285	1.000	39	0
Risk_O	unc005_k25	Unknown	10	58	40	3.637	1.000	35	<0.001
Risk_O	unc005_k25	Right Cerebellum Exterior	32	-46	-28	3.752	0.999	32	<0.001
Risk_O	unc005_k25	Brain Stem	4	-26	-38	3.227	1.000	26	<0.001

Risk_O	unc005_k25	Right Cerebral White Matter	46	-50	26	3.271	1.000	25	<0.001
Risk_O	unc005_k25	Right PoG postcentral gyrus	60	-16	40	3.199	1.000	25	<0.001
Risk_O	unc005_k25	Unknown	2	38	56	3.184	1.000	25	<0.001
Pain_S	FWE_p05	Left AIns anterior insula	-42	6	-6	8.862	2.70851030531594e-05	1819	NaN
Pain_S	FWE_p05	Right AIns anterior insula	36	8	8	7.867	0.000	1097	NaN
Pain_S	FWE_p05	Left MCgG middle cingulate gyrus	0	8	34	9.800	3.37782245241058e-06	920	NaN
Pain_S	FWE_p05	Left Cerebral White Matter	-54	-30	30	8.230	0.000	395	NaN
Pain_S	FWE_p05	Right PO parietal operculum	58	-28	26	7.435	0.001	303	NaN
Pain_S	FWE_p05	Left Cerebral White Matter	-8	-16	70	7.316	0.001	122	0
Pain_S	FWE_p05	Left SPL superior parietal lobule	-18	-48	66	6.861	0.003	88	0
Pain_S	FWE_p05	Unknown	6	-36	0	6.963	0.002	65	0
Pain_S	FWE_p05	Right Cerebral White Matter	14	-6	68	7.521	0.001	61	0
Pain_S	FWE_p05	Right Thalamus Proper	6	-10	6	6.291	0.012	51	0
Pain_S	FWE_p05	Right Cerebellum White Matter	20	-46	-48	6.802	0.003	25	0
Pain_S	FWE_p05	Right CO central operculum	56	-12	18	6.065	0.020	12	0
Pain_S	FWE_p05	Left Thalamus Proper	-8	-8	10	6.040	0.021	11	0
Pain_S	FWE_p05	Right TrIFG triangular part of the inferior frontal gyrus	46	38	6	6.194	0.015	9	0
Pain_S	FWE_p05	Unknown	4	-8	78	5.777	0.040	3	0
Pain_S	unc005_k25	Left MCgG middle cingulate gyrus	0	8	34	9.800	3.37782245241058e-06	43582	NaN
Pain_S	unc005_k25	Right PrG precentral gyrus	36	-6	52	3.991	0.913	267	0
Pain_S	unc005_k25	Right Cerebellum	32	-64	-22	4.037	0.892	191	0

		Exterior							
Pain_S	unc005_k25	Left PrG precentral gyrus	-38	-8	48	4.256	0.750	159	0
Pain_S	unc005_k25	Left MTG middle temporal gyrus	-50	-62	8	4.329	0.694	152	0
Pain_O	unc005_k25	Unknown	62	16	12	4.174	0.804	679	0
Pain_O	unc005_k25	Right SMC supplementary motor cortex	8	12	60	4.709	0.390	657	0
Pain_O	unc005_k25	Left IOG inferior occipital gyrus	-30	-98	2	4.752	0.361	441	0
Pain_O	unc005_k25	Right PrG precentral gyrus	50	4	50	5.052	0.200	439	0
Pain_O	unc005_k25	Right Cerebral White Matter	22	-96	-4	4.504	0.545	432	0
Pain_O	unc005_k25	Left Cerebellum Exterior	-34	-54	-30	4.008	0.901	162	0
Pain_O	unc005_k25	Right PrG precentral gyrus	48	8	22	3.195	1.000	129	0
Pain_O	unc005_k25	Brain Stem	6	-30	-24	3.426	0.999	39	0
Pain_O	unc005_k25	Left SMG supramarginal gyrus	-62	-40	44	3.140	1.000	39	0
Pain_O	unc005_k25	Left Cerebral White Matter	-34	-6	42	3.135	1.000	38	0
Pain_O	unc005_k25	Left Cerebral White Matter	-30	20	0	3.305	1.000	29	<0.001
PainPE_S	unc005_k25	Left Pallidum	-12	2	-2	3.674	0.997	59	0
PainPE_S	unc005_k25	Right PP planum polare	44	-2	-16	4.155	0.882	52	0
PainPE_S	unc005_k25	Left Cerebral White Matter	-24	-88	-8	3.135	1.000	39	0
PainPE_S	unc005_k25	Right POrG posterior orbital gyrus	26	16	-18	3.349	1.000	26	<0.001
PainPE_O	unc005_k25	Left Cerebellum Exterior	-4	-48	-44	4.293	0.690	77	0
PainPE_O	unc005_k25	Unknown	56	36	18	3.657	0.988	40	0
Surp_S	unc005_k25	Right PrG precentral gyrus	24	-12	58	4.853	0.403	2197	0
Surp_S	unc005_k25	Left Cerebral	-44	-50	26	5.500	0.107	447	0

		White Matter							
Surp_S	unc005_k25	Right Lateral Ventricle	6	-14	20	4.449	0.725	268	0
Surp_S	unc005_k25	Unknown	-8	-100	-14	4.004	0.966	187	0
Surp_S	unc005_k25	Left ACgG anterior cingulate gyrus	0	46	-4	3.253	1.000	167	0
Surp_S	unc005_k25	Left Cerebral White Matter	-16	-34	58	3.754	0.996	155	0
Surp_S	unc005_k25	Right AnG angular gyrus	60	-46	30	3.590	1.000	149	0
Surp_S	unc005_k25	Right MOG middle occipital gyrus	36	-88	12	3.527	1.000	147	0
Surp_S	unc005_k25	Left SMC supplementary motor cortex	-2	6	68	3.279	1.000	137	0
Surp_S	unc005_k25	Cerebellar Vermal Lobules I-V	-6	-50	-4	3.947	0.978	123	0
Surp_S	unc005_k25	Right Cerebellum Exterior	46	-72	-44	3.880	0.987	121	0
Surp_S	unc005_k25	Left SFG superior frontal gyrus	-8	46	50	3.697	0.998	119	0
Surp_S	unc005_k25	Unknown	44	26	-22	4.505	0.680	118	0
Surp_S	unc005_k25	Right MPrG precentral gyrus medial segment	6	-28	52	3.152	1.000	116	0
Surp_S	unc005_k25	Left TMP temporal pole	-42	20	-28	3.550	1.000	98	0
Surp_S	unc005_k25	Right Cerebral White Matter	38	-52	30	3.953	0.977	89	0
Surp_S	unc005_k25	Unknown	60	26	18	3.953	0.977	82	0
Surp_S	unc005_k25	Right SFG superior frontal gyrus	12	54	38	3.816	0.993	79	0
Surp_S	unc005_k25	Left MOG middle occipital gyrus	-34	-92	16	3.623	0.999	72	0
Surp_S	unc005_k25	Left MSFG superior frontal gyrus medial segment	-6	56	32	3.484	1.000	71	0
Surp_S	unc005_k25	Right MTG middle	48	-28	-4	3.370	1.000	69	0

		temporal gyrus							
Surp_S	unc005_k25	Left Ventral DC	-16	-26	-10	3.231	1.000	66	0
Surp_S	unc005_k25	Left Amygdala	-18	-6	-14	3.479	1.000	63	0
Surp_S	unc005_k25	Left AnG angular gyrus	-42	-74	44	3.188	1.000	63	0
Surp_S	unc005_k25	Right Cerebral White Matter	22	-8	-12	3.848	0.991	59	0
Surp_S	unc005_k25	Right SFG superior frontal gyrus	22	32	58	3.455	1.000	50	0
Surp_S	unc005_k25	Left Cerebellum Exterior	-28	-42	-28	3.660	0.999	44	0
Surp_S	unc005_k25	Left Cerebral White Matter	-18	-68	32	3.203	1.000	44	0
Surp_S	unc005_k25	Left PCu precuneus	0	-56	34	2.995	1.000	44	0
Surp_S	unc005_k25	Unknown	6	-88	-22	3.059	1.000	39	0
Surp_S	unc005_k25	Unknown	22	6	-20	3.934	0.980	38	0
Surp_S	unc005_k25	Right PrG precentral gyrus	60	4	10	3.408	1.000	38	0
Surp_S	unc005_k25	Left Cerebral White Matter	-8	-14	38	3.326	1.000	38	0
Surp_S	unc005_k25	Left Cerebral White Matter	-8	22	60	3.259	1.000	36	0
Surp_S	unc005_k25	Right OCP occipital pole	20	-98	-4	3.120	1.000	34	<0.001
Surp_S	unc005_k25	Unknown	38	62	14	3.549	1.000	33	<0.001
Surp_S	unc005_k25	Right Hippocampus	24	-24	-10	3.238	1.000	32	<0.001
Surp_S	unc005_k25	Left FO frontal operculum	-42	18	-2	3.082	1.000	32	<0.001
Surp_S	unc005_k25	Right Thalamus Proper	12	-32	-2	4.294	0.837	30	<0.001
Surp_S	unc005_k25	Left SFG superior frontal gyrus	-22	24	60	3.263	1.000	30	<0.001
Surp_O	unc005_k25	Left ACgG anterior cingulate gyrus	-2	36	6	3.489	0.999	219	0
Surp_O	unc005_k25	Right TrIFG triangular part of the inferior	44	28	2	3.944	0.930	210	0

		frontal gyrus							
Surp_O	unc005_k25	Left Cerebral White Matter	-4	12	-6	3.351	1.000	78	0
Ratings_S	unc005_k25	Right PrG precentral gyrus	40	6	32	3.355	1.000	138	0
Ratings_S	unc005_k25	Right SPL superior parietal lobule	24	-68	52	3.404	0.999	81	0
Ratings_S	unc005_k25	Right MFG middle frontal gyrus	46	48	14	3.696	0.985	63	0
Ratings_S	unc005_k25	Unknown	50	6	54	3.503	0.998	51	0
Ratings_S	unc005_k25	Right Cerebral White Matter	32	40	-4	4.032	0.877	36	0
Ratings_O	unc005_k25	Right MFG middle frontal gyrus	48	28	32	4.582	0.470	245	0
Ratings_O	unc005_k25	Right SMG supramarginal gyrus	56	-36	56	4.354	0.653	52	0
Ratings_O	unc005_k25	Left MFG middle frontal gyrus	-42	30	40	3.524	0.997	33	<0.001

S6. Beta extraction within ROIs

Table S6.1 Full results of beta extraction values within ROIs.

Contrast	ROI	Mean	SE	T	df	p	N	Sig
EP_S	ACC_L	-0.358	0.121	-2.951	32	0 6	33	**
EP_S	ACC_R	-0.364	0.139	-2.615	32	0.014	33	*
EP_S	AIns_L	-0.047	0.178	-0.262	32	0.795	33	
EP_S	AIns_R	-0.151	0.179	-0.843	32	0.405	33	
EP_S	Caud_L	-0.277	0.154	-1.795	32	0.082	33	
EP_S	Caud_R	-0.241	0.136	-1.771	32	0.086	33	
EP_S	Put_L	-0.304	0.163	-1.864	32	0.072	33	
EP_S	Put_R	-0.271	0.158	-1.718	32	0.095	33	
EP_O	ACC_L	-0.010	0.141	-0.074	32	0.941	33	
EP_O	ACC_R	-0.060	0.139	-0.433	32	0.668	33	
EP_O	AIns_L	0.128	0.119	1.083	32	0.287	33	
EP_O	AIns_R	0.007	0.099	0.067	32	0.947	33	
EP_O	Caud_L	0.133	0.113	1.183	32	0.246	33	
EP_O	Caud_R	0.037	0.107	0.347	32	0.731	33	
EP_O	Put_L	-0.061	0.094	-0.650	32	0.520	33	
EP_O	Put_R	-0.024	0.098	-0.240	32	0.812	33	

Risk_S	ACC_L	0.051	0.231	0.220	32	0.827	33	
Risk_S	ACC_R	-0.040	0.248	-0.161	32	0.873	33	
Risk_S	AIns_L	-0.081	0.172	-0.469	32	0.642	33	
Risk_S	AIns_R	-0.228	0.172	-1.326	32	0.194	33	
Risk_S	Caud_L	0.225	0.145	1.548	32	0.131	33	
Risk_S	Caud_R	0.103	0.132	0.778	32	0.442	33	
Risk_S	Put_L	0.008	0.154	0.053	32	0.958	33	
Risk_S	Put_R	-0.071	0.161	-0.444	32	0.660	33	
Risk_O	ACC_L	0.247	0.226	1.094	32	0.282	33	
Risk_O	ACC_R	0.104	0.208	0.502	32	0.619	33	
Risk_O	AIns_L	0.367	0.114	3.214	32	0 3	33	**
Risk_O	AIns_R	0.305	0.132	2.315	32	0.027	33	*
Risk_O	Caud_L	0.478	0.161	2.964	32	0.006	33	**
Risk_O	Caud_R	0.358	0.145	2.469	32	0.019	33	*
Risk_O	Put_L	0.531	0.142	3.731	32	0.001	33	***
Risk_O	Put_R	0.421	0.123	3.421	32	0.002	33	**
PainPE_S	ACC_L	0.255	0.455	0.561	32	0.579	33	
PainPE_S	ACC_R	0.463	0.456	1.016	32	0.317	33	
PainPE_S	AIns_L	0.327	0.362	0.905	32	0.372	33	
PainPE_S	AIns_R	0.685	0.346	1.984	32	0.056	33	
PainPE_S	Caud_L	0.637	0.300	2.125	32	0.041	33	*
PainPE_S	Caud_R	0.474	0.281	1.684	32	0.102	33	
PainPE_S	Put_L	0.444	0.296	1.503	32	0.143	33	
PainPE_S	Put_R	0.515	0.307	1.676	32	0.104	33	
PainPE_O	ACC_L	0.021	0.110	0.196	32	0.846	33	
PainPE_O	ACC_R	0.046	0.108	0.428	32	0.672	33	
PainPE_O	AIns_L	0.050	0.087	0.578	32	0.567	33	
PainPE_O	AIns_R	0.062	0.079	0.784	32	0.439	33	
PainPE_O	Caud_L	-0.067	0.080	-0.841	32	0.407	33	
PainPE_O	Caud_R	-0.024	0.081	-0.299	32	0.767	33	
PainPE_O	Put_L	-0.020	0.078	-0.260	32	0.797	33	
PainPE_O	Put_R	-0.015	0.074	-0.203	32	0.840	33	
Surp_S	ACC_L	0.250	0.239	1.048	32	0.302	33	
Surp_S	ACC_R	0.224	0.253	0.883	32	0.384	33	
Surp_S	AIns_L	0.184	0.148	1.238	32	0.225	33	
Surp_S	AIns_R	0.212	0.161	1.318	32	0.197	33	
Surp_S	Caud_L	0.210	0.180	1.171	32	0.250	33	
Surp_S	Caud_R	0.255	0.160	1.597	32	0.120	33	
Surp_S	L_AIns_Surp_CC_NII	0.009	0.157	0.057	32	0.955	33	
Surp_S	Put_L	0.174	0.157	1.104	32	0.278	33	
Surp_S	Put_R	0.149	0.169	0.878	32	0.387	33	
Surp_S	R_AIns_Surp_CC_NII	0.371	0.168	2.207	32	0.035	33	*

Surp_O	ACC_L	0.047	0.081	0.583	32	0.564	33	
Surp_O	ACC_R	0.082	0.076	1.080	32	0.288	33	
Surp_O	AIns_L	0.069	0.063	1.092	32	0.283	33	
Surp_O	AIns_R	0.051	0.052	0.981	32	0.334	33	
Surp_O	Caud_L	-0.011	0.049	-0.219	32	0.828	33	
Surp_O	Caud_R	-0.038	0.046	-0.830	32	0.413	33	
Surp_O	L_AIns_Surp_CC_NII	0.051	0.047	1.079	32	0.288	33	
Surp_O	Put_L	-0.014	0.050	-0.290	32	0.774	33	
Surp_O	Put_R	0.005	0.052	0.087	32	0.931	33	
Surp_O	R_AIns_Surp_CC_NII	0.150	0.073	2.065	32	0.047	33	*
EP_SvsO	ACC_L	-0.347	0.167	-2.080	32	0.046	33	*
EP_SvsO	ACC_R	-0.304	0.186	-1.631	32	0.113	33	
EP_SvsO	AIns_L	-0.175	0.215	-0.813	32	0.422	33	
EP_SvsO	AIns_R	-0.157	0.212	-0.742	32	0.464	33	
EP_SvsO	Caud_L	-0.411	0.175	-2.342	32	0.026	33	*
EP_SvsO	Caud_R	-0.279	0.172	-1.625	32	0.114	33	
EP_SvsO	Put_L	-0.243	0.172	-1.414	32	0.167	33	
EP_SvsO	Put_R	-0.248	0.169	-1.466	32	0.152	33	
Risk_SvsO	ACC_L	-0.196	0.337	-0.582	32	0.565	33	
Risk_SvsO	ACC_R	-0.144	0.346	-0.417	32	0.679	33	
Risk_SvsO	AIns_L	-0.448	0.225	-1.993	32	0.055	33	
Risk_SvsO	AIns_R	-0.533	0.226	-2.357	32	0.025	33	*
Risk_SvsO	Caud_L	-0.253	0.217	-1.165	32	0.253	33	
Risk_SvsO	Caud_R	-0.255	0.204	-1.249	32	0.221	33	
Risk_SvsO	Put_L	-0.523	0.243	-2.148	32	0.039	33	*
Risk_SvsO	Put_R	-0.492	0.225	-2.191	32	0.036	33	*
PainPE_SvsO	ACC_L	0.234	0.477	0.491	32	0.627	33	
PainPE_SvsO	ACC_R	0.417	0.480	0.868	32	0.392	33	
PainPE_SvsO	AIns_L	0.277	0.370	0.750	32	0.459	33	
PainPE_SvsO	AIns_R	0.623	0.359	1.738	32	0.092	33	
PainPE_SvsO	Caud_L	0.705	0.318	2.216	32	0.034	33	*
PainPE_SvsO	Caud_R	0.498	0.300	1.662	32	0.106	33	
PainPE_SvsO	Put_L	0.464	0.312	1.488	32	0.146	33	
PainPE_SvsO	Put_R	0.530	0.323	1.638	32	0.111	33	
Surp_SvsO	ACC_L	0.203	0.273	0.742	32	0.464	33	
Surp_SvsO	ACC_R	0.141	0.272	0.519	32	0.607	33	
Surp_SvsO	AIns_L	0.115	0.149	0.769	32	0.447	33	
Surp_SvsO	AIns_R	0.161	0.165	0.974	32	0.337	33	
Surp_SvsO	Caud_L	0.221	0.186	1.188	32	0.244	33	
Surp_SvsO	Caud_R	0.294	0.167	1.758	32	0.088	33	
Surp_SvsO	L_AIns_Surp_CC_NII	-0.042	0.163	-0.256	32	0.800	33	
Surp_SvsO	Put_L	0.188	0.164	1.143	32	0.261	33	

Surp_SvsO	Put_R	0.144	0.174	0.827	32	0.415	33	
Surp_SvsO	R_AIns_Surp_CC_NII	0.221	0.182	1.218	32	0.232	33	

S7. RSA results – Predictive Inference

Table S7.1 Full RSA results for all prediction variables in all ROIs

ROI	Variable	n	Self_mean	Self_t	Self_p	Self_wilc	Self_perm_sig	Other_mean	Other_t	Other_p	Other_wilc	Other_perm_sig	Diff_t	Diff_p	Diff_wilcoxon
ACC_L	EP	33	-0.016	-0.984	0.332	0.321	1.0	-0.003	-0.185	0.854	0.525	2.0	-0.532	0.598	0.480
ACC_R	EP	33	0.013	0.838	0.408	0.480	1.0	-0.002	-0.148	0.883	0.819	0.0	0.718	0.478	0.458
AIns_L	EP	33	-0.008	-0.496	0.623	0.698	1.0	0.001	0.057	0.955	0.609	0.0	-0.398	0.693	0.916
AIns_R	EP	33	0.003	0.174	0.863	1.000	3.0	-0.005	-0.290	0.773	0.805	2.0	0.423	0.675	0.930
Caud_L	EP	33	-0.016	-1.230	0.227	0.208	0.0	0.035	1.896	0.067	0.068	2.0	-2.192	0.036	0.035
Caud_R	EP	33	-0.002	-0.135	0.893	0.376	1.0	0.009	0.475	0.638	0.888	4.0	-0.499	0.621	0.560
Put_L	EP	33	-0.003	-0.182	0.857	0.659	1.0	0.007	0.389	0.700	0.944	3.0	-0.490	0.627	0.646
Put_R	EP	33	-0.017	-1.123	0.270	0.135	1.0	0.002	0.117	0.907	0.846	3.0	-0.907	0.371	0.437
ACC_L	Risk	33	-0.007	-0.428	0.672	0.502	1.0	0.026	1.463	0.153	0.208	4.0	-1.376	0.178	0.208
ACC_R	Risk	33	-0.027	-1.858	0.072	0.046	0.0	0.029	1.590	0.122	0.257	3.0	-2.347	0.025	0.014
AIns_L	Risk	33	-0.002	-0.114	0.910	0.711	1.0	0.030	1.777	0.085	0.086	4.0	-1.289	0.207	0.201
AIns_R	Risk	33	0.011	0.768	0.448	0.698	3.0	0.001	0.072	0.943	0.860	1.0	0.523	0.604	0.944
Caud_L	Risk	33	-0.006	-0.447	0.658	0.406	2.0	-0.007	-0.490	0.628	0.491	0.0	0.032	0.975	0.874
Caud_R	Risk	33	-0.011	-0.712	0.481	0.396	1.0	-0.014	-1.066	0.294	0.150	1.0	0.185	0.855	0.805
Put_L	Risk	33	-0.004	-0.285	0.777	0.502	2.0	0.004	0.232	0.818	0.832	1.0	-0.332	0.742	0.916
Put_R	Risk	33	-0.016	-0.980	0.335	0.288	2.0	-0.002	-0.107	0.916	0.751	2.0	-0.896	0.377	0.330

S8. RSA results – Post Outcome Update

Table S8.1 Full RSA results for all prediction error variables in all ROIs

ROI	Variable	n	Self_mean	Self_t	Self_p	Self_wilc	Self_perm_sig	Other_mean	Other_t	Other_p	Other_wilc	Other_perm_sig	Diff_t	Diff_p	Diff_wilcoxon
ACC_L	Signed PE	33	0.032	1.501	0.143	0.367	5.000	0.012	0.689	0.496	0.672	2.000	0.712	0.482	0.386
ACC_R	Signed PE	33	0.041	1.908	0.065	0.121	3.000	0.024	1.292	0.206	0.358	3.000	0.607	0.548	0.596
AIns_L	Signed PE	33	0.059	3.121	0.004	0.004	7.000	0.054	3.164	0.003	0.008	6.000	0.168	0.867	0.819
AIns_R	Signed PE	33	0.068	3.270	0.003	0.006	7.000	0.048	2.716	0.011	0.014	3.000	0.855	0.399	0.584
Caud_L	Signed PE	33	0.016	1.041	0.306	0.339	1.000	0.003	0.191	0.850	0.791	1.000	0.533	0.598	0.525
Caud_R	Signed PE	33	0.042	2.474	0.019	0.039	4.000	0.046	2.427	0.021	0.046	5.000	-0.177	0.861	1.000
Put_L	Signed PE	33	0.034	1.538	0.134	0.272	4.000	0.015	0.915	0.367	0.584	2.000	0.634	0.531	0.791
Put_R	Signed PE	33	0.032	1.514	0.140	0.406	5.000	0.033	1.574	0.125	0.339	4.000	-0.042	0.967	0.724
ACC_L	Surprise	33	-0.023	-1.505	0.142	0.130	0.000	-0.014	-0.746	0.461	0.621	1.000	-0.356	0.725	0.572
ACC_R	Surprise	33	-0.020	-1.218	0.232	0.165	0.000	-0.005	-0.353	0.726	0.584	1.000	-0.589	0.560	0.560
AIns_L	Surprise	33	-0.013	-0.839	0.407	0.634	0.000	0.014	0.722	0.476	0.525	2.000	-1.108	0.276	0.386
AIns_R	Surprise	33	-0.021	-1.153	0.258	0.140	1.000	0.016	0.701	0.488	0.698	5.000	-1.175	0.249	0.235
Caud_L	Surprise	33	0.009	0.549	0.587	0.832	4.000	-0.018	-1.061	0.297	0.396	0.000	1.316	0.198	0.214
Caud_R	Surprise	33	0.009	0.486	0.630	0.609	2.000	0.008	0.396	0.695	0.596	1.000	0.051	0.960	0.916
Put_L	Surprise	33	-0.026	-1.553	0.130	0.051	2.000	0.011	0.599	0.553	0.437	1.000	-1.402	0.171	0.177
Put_R	Surprise	33	-0.012	-0.994	0.328	0.264	1.000	0.029	1.541	0.133	0.358	5.000	-1.836	0.076	0.150

S9. Encoding model results - Predictive Inference

Table S9.1 Full encoding results for all prediction variables in all ROIs

Variable	ROI	n	Self_mean	Self_t	Self_p	Other_mean	Other_t	Other_p	Diff_t	Diff_p	Diff_wilcoxon
EP	ACC_L	33	-0.056	-1.667	0.105	0.009	0.289	0.775	-1.546	0.132	0.257
EP	ACC_R	33	-0.051	-1.307	0.201	-0.007	-0.211	0.834	-0.906	0.372	0.396
EP	AIns_L	33	0.002	0.054	0.958	-0.009	-0.303	0.764	0.210	0.835	0.596
EP	AIns_R	33	-0.015	-0.302	0.765	-0.001	-0.037	0.970	-0.237	0.814	0.846
EP	Caud_L	33	-0.095	-2.582	0.015	-0.005	-0.155	0.878	-2.119	0.042	0.083

EP	Caud_R	33	-0.073	-1.979	0.056	-0.006	-0.212	0.833	-1.803	0.081	0.144
EP	Put_L	33	-0.068	-1.545	0.132	-0.060	-1.848	0.074	-0.135	0.893	0.986
EP	Put_R	33	-0.068	-1.554	0.130	-0.064	-2.060	0.048	-0.082	0.935	0.902
Risk	ACC_L	33	0.041	1.048	0.302	0.069	2.258	0.031	-0.512	0.612	0.537
Risk	ACC_R	33	0.017	0.407	0.687	0.046	1.510	0.141	-0.512	0.612	0.537
Risk	AIns_L	33	-0.003	-0.070	0.944	0.057	2.075	0.046	-1.291	0.206	0.280
Risk	AIns_R	33	-0.029	-0.757	0.455	0.067	2.160	0.038	-1.959	0.059	0.060
Risk	Caud_L	33	0.010	0.291	0.773	0.079	2.508	0.017	-1.686	0.101	0.121
Risk	Caud_R	33	0.002	0.063	0.950	0.067	2.134	0.041	-1.556	0.130	0.126
Risk	Put_L	33	-0.001	-0.031	0.975	0.084	2.932	0.006	-1.700	0.099	0.121
Risk	Put_R	33	-0.026	-0.701	0.488	0.078	2.697	0.011	-2.289	0.029	0.034

S10. Encoding model results - Post Outcome Update

Table S10.1 Full encoding results for all prediction error variables in all ROIs

Variable	ROI	n	Self_mean	Self_t	Self_p	Other_mean	Other_t	Other_p	Diff_t	Diff_p	Diff_wilcoxon
SignedPE	ACC_L	33	0.086	1.537	0.134	-0.014	-0.301	0.765	1.255	0.218	0.264
SignedPE	ACC_R	33	0.124	2.377	0.024	-0.004	-0.079	0.938	1.638	0.111	0.160
SignedPE	AIns_L	33	0.291	6.727	0.000	0.100	2.273	0.030	2.856	0.007	0.008
SignedPE	AIns_R	33	0.317	6.763	0.000	0.125	2.916	0.006	2.785	0.009	0.005
SignedPE	Caud_L	33	0.120	2.727	0.010	-0.062	-1.572	0.126	2.976	0.006	0.003
SignedPE	Caud_R	33	0.119	2.798	0.009	-0.033	-0.881	0.385	2.618	0.013	0.012
SignedPE	Put_L	33	0.161	3.143	0.004	0.016	0.374	0.711	2.057	0.048	0.063
SignedPE	Put_R	33	0.124	2.283	0.029	-0.003	-0.075	0.941	1.696	0.100	0.280
Surprise	ACC_L	33	0.054	1.371	0.180	-0.005	-0.118	0.907	0.890	0.380	0.280
Surprise	ACC_R	33	0.063	1.489	0.146	0.005	0.142	0.888	0.875	0.388	0.242
Surprise	AIns_L	33	0.097	2.247	0.032	0.012	0.252	0.803	1.200	0.239	0.249
Surprise	AIns_R	33	0.097	1.956	0.059	0.024	0.610	0.546	1.030	0.311	0.235
Surprise	Caud_L	33	0.043	1.062	0.296	-0.023	-0.600	0.553	1.023	0.314	0.264
Surprise	Caud_R	33	0.051	1.359	0.184	-0.060	-1.643	0.110	1.885	0.069	0.041
Surprise	Put_L	33	0.064	1.494	0.145	-0.050	-1.225	0.229	1.683	0.102	0.027
Surprise	Put_R	33	0.058	1.366	0.181	-0.048	-1.122	0.270	1.522	0.138	0.018

S11. Full results of whole brain analyses – objective regressors

Table S11.1 Full univariate results for all contrasts, whole brain

1

Contrast	Threshold	Region	X	Y	Z	peak_T	peak_pFWE	k_voxels	cluster_pFWE
EP_S	unc005_k25	Right SOG superior occipital gyrus	24	-92	18	3.128	1	86	0
EP_S	unc005_k25	Unknown	-40	54	18	3.180	1	42	0
EP_S	unc005_k25	Left SFG superior frontal gyrus	-20	0	64	3.388	1	37	0
EP_O	FWE_p05	Right Cerebral White Matter	18	-96	12	7.368	0.002	232	0
EP_O	FWE_p05	Left OFuG occipital fusiform gyrus	-26	-80	-10	6.375	0.017	13	0
EP_O	FWE_p05	Right Cerebral White Matter	30	-68	-10	6.675	0.008	11	0
EP_O	FWE_p05	Right FuG fusiform gyrus	28	-48	-16	7.017	0.004	10	0
EP_O	unc005_k25	Right Cerebral White Matter	18	-96	12	7.368	0.002	3032	NaN
EP_O	unc005_k25	Left OFuG occipital fusiform gyrus	-26	-80	-10	6.375	0.017	2807	NaN
EP_O	unc005_k25	Left SMC supplementary motor cortex	-4	14	42	4.757	0.544	1067	0
EP_O	unc005_k25	Right Lateral Ventricle	14	-30	18	4.304	0.885	84	0
EP_O	unc005_k25	Right Cerebral White Matter	24	-12	50	3.752	0.999	39	0
EP_O	unc005_k25	Left MFG middle frontal gyrus	-32	38	32	3.458	1	36	0
EP_O	unc005_k25	Left Cerebral White Matter	-48	-20	34	3.465	1	33	<.001
EP_O	unc005_k25	Left Cerebral White Matter	-26	-62	10	3.659	1	26	<.001
EP_O	unc005_k25	Left SPL superior parietal lobule	-14	-66	66	3.268	1	26	<.001
Risk_S	unc005_k25	Right Cerebral White Matter	14	-86	-6	5.467	0.111	456	0
Risk_S	unc005_k25	Left Cerebral White Matter	-18	-96	10	3.630	0.999	209	0
Risk_S	unc005_k25	Right Cerebral White Matter	36	-34	4	4.202	0.883	176	0
Risk_S	unc005_k25	Unknown	-16	8	74	3.597	0.999	127	0
Risk_S	unc005_k25	Right Cerebral White Matter	26	-24	36	4.537	0.641	125	0
Risk_S	unc005_k25	Left Cerebellum Exterior	-48	-44	-44	4.167	0.901	121	0
Risk_S	unc005_k25	Left Lateral Ventricle	-20	-38	20	3.547	1	96	0
Risk_S	unc005_k25	Right SPL superior parietal lobule	18	-68	54	3.470	1	82	0
Risk_S	unc005_k25	Left Caudate	-16	18	12	3.967	0.971	75	0
Risk_S	unc005_k25	Left SMC supplementary motor cortex	-6	20	44	3.702	0.998	74	0
Risk_S	unc005_k25	Left Cerebral White Matter	-50	-10	20	4.302	0.822	72	0

Risk_S	unc005_k25	Unknown	12	-26	82	4.296	0.826	65	0
Risk_S	unc005_k25	Left Cerebral White Matter	-40	28	30	3.746	0.996	60	0
Risk_S	unc005_k25	Right Cerebellum Exterior	38	-46	-34	3.374	1	55	0
Risk_S	unc005_k25	Left Cerebral White Matter	-16	-6	34	3.954	0.973	54	0
Risk_S	unc005_k25	Left SPL superior parietal lobule	-10	-72	60	3.207	1	50	0
Risk_S	unc005_k25	Left Cerebral White Matter	-20	-32	38	4.234	0.865	45	0
Risk_S	unc005_k25	Left Lateral Ventricle	-10	2	22	4.220	0.873	39	0
Risk_S	unc005_k25	Left Cerebral White Matter	-32	46	12	3.114	1	38	0
Risk_S	unc005_k25	Left Cerebral White Matter	-26	40	6	3.158	1	34	<.001
Risk_O	unc005_k25	Right Thalamus Proper	12	-14	0	5.537	0.099	19279	NaN
Risk_O	unc005_k25	Left SPL superior parietal lobule	-14	-68	52	4.505	0.685	1085	0
Risk_O	unc005_k25	Left TMP temporal pole	-48	10	-36	4.996	0.313	805	0
Risk_O	unc005_k25	Right Ent entorhinal area	22	2	-34	4.042	0.958	478	0
Risk_O	unc005_k25	Left Cerebral White Matter	-30	-40	48	5.036	0.289	289	0
Risk_O	unc005_k25	Right Cerebellum Exterior	38	-50	-52	4.153	0.918	256	0
Risk_O	unc005_k25	Left MFG middle frontal gyrus	-36	44	20	4.402	0.766	207	0
Risk_O	unc005_k25	Right Cerebral White Matter	46	-20	-24	3.479	1	148	0
Risk_O	unc005_k25	Left Cerebellum Exterior	-14	-62	-48	4.481	0.704	103	0
Risk_O	unc005_k25	Left Cerebral White Matter	-40	28	30	3.391	1	82	0
Risk_O	unc005_k25	Right Cerebral White Matter	6	-36	22	5.022	0.298	79	0
Risk_O	unc005_k25	Left PrG precentral gyrus	-38	-18	42	3.503	1	74	0
Risk_O	unc005_k25	Right TMP temporal pole	56	10	-12	3.771	0.996	54	0
Risk_O	unc005_k25	Left TrIFG triangular part of the inferior frontal gyrus	-52	32	-4	3.102	1	45	0
Risk_O	unc005_k25	Left Cerebral White Matter	-46	-6	-32	3.231	1	44	0
Risk_O	unc005_k25	Left Cerebral White Matter	-46	-44	30	3.580	1	43	0
Risk_O	unc005_k25	Brain Stem	4	-24	-42	3.166	1	39	0
Risk_O	unc005_k25	Right Cerebral White Matter	22	-20	34	4.059	0.953	35	<.001
Risk_O	unc005_k25	Left ITG inferior temporal gyrus	-62	-18	-30	3.294	1	28	<.001
Risk_O	unc005_k25	Left Cerebral White Matter	-34	-70	28	3.070	1	25	<.001

PainPE_S	unc005_k25	Right Cerebral White Matter	38	-22	-20	3.534	0.998	151	0
PainPE_S	unc005_k25	Unknown	44	2	-12	3.922	0.941	132	0
PainPE_S	unc005_k25	Right Thalamus Proper	8	-8	-4	3.630	0.994	99	0
PainPE_S	unc005_k25	Right PHG parahippocampal gyrus	14	-34	-10	3.440	0.999	77	0
PainPE_S	unc005_k25	Left Cerebral White Matter	-24	-92	-10	3.383	1	65	0
PainPE_S	unc005_k25	Left Pallidum	-12	2	-2	3.333	1	39	0
PainPE_O	unc005_k25	Unknown	-8	-6	-16	3.956	0.882	47	0
Surp_S	unc005_k25	Right PoG postcentral gyrus	28	-38	58	4.722	0.482	1344	0
Surp_S	unc005_k25	Left SPL superior parietal lobule	-20	-46	68	4.240	0.855	639	0
Surp_S	unc005_k25	Left Cerebral White Matter	-52	-50	24	3.920	0.978	482	0
Surp_S	unc005_k25	Left SFG superior frontal gyrus	-8	24	64	4.179	0.889	460	0
Surp_S	unc005_k25	Unknown	54	36	-12	4.375	0.762	450	0
Surp_S	unc005_k25	Left PCu precuneus	-2	-54	44	4.242	0.854	444	0
Surp_S	unc005_k25	Unknown	-52	30	-12	4.190	0.884	367	0
Surp_S	unc005_k25	Unknown	6	-98	-8	3.978	0.966	351	0
Surp_S	unc005_k25	Right PoG postcentral gyrus	62	-6	28	3.998	0.961	302	0
Surp_S	unc005_k25	Right SFG superior frontal gyrus	12	16	66	3.659	0.998	291	0
Surp_S	unc005_k25	Right Lateral Ventricle	6	-14	22	4.011	0.957	165	0
Surp_S	unc005_k25	Unknown	4	-98	18	3.724	0.997	163	0
Surp_S	unc005_k25	Right Cerebral White Matter	28	-40	26	3.922	0.977	141	0
Surp_S	unc005_k25	Right Cerebral White Matter	54	-42	-2	3.591	0.999	124	0
Surp_S	unc005_k25	Brain Stem	6	-20	-26	3.884	0.983	114	0
Surp_S	unc005_k25	Right Cerebellum Exterior	34	-84	-34	3.729	0.996	101	0
Surp_S	unc005_k25	Left Cerebral White Matter	-14	-22	46	3.645	0.999	74	0
Surp_S	unc005_k25	Left Cerebral White Matter	-18	0	-12	3.592	0.999	73	0
Surp_S	unc005_k25	Left SFG superior frontal gyrus	-24	26	60	3.532	1	67	0
Surp_S	unc005_k25	Left Cerebellum Exterior	-50	-66	-32	3.507	1	66	0
Surp_S	unc005_k25	Left Cerebellum Exterior	-32	-58	-26	3.360	1	63	0
Surp_S	unc005_k25	Unknown	0	46	-14	3.687	0.998	63	0
Surp_S	unc005_k25	Right Lateral Ventricle	12	-28	20	3.721	0.997	61	0

Surp_S	unc005_k25	Unknown	0	-22	48	3.198	1	56	0
Surp_S	unc005_k25	Right AnG angular gyrus	60	-46	30	3.287	1	55	0
Surp_S	unc005_k25	Left Cerebral White Matter	-18	-78	22	3.082	1	49	0
Surp_S	unc005_k25	Right Cerebellum Exterior	22	-74	-18	3.084	1	47	0
Surp_S	unc005_k25	Right TMP temporal pole	46	10	-42	3.327	1	45	0
Surp_S	unc005_k25	Left SFG superior frontal gyrus	-20	50	38	3.298	1	41	0
Surp_S	unc005_k25	Right Cerebral White Matter	8	-12	60	3.359	1	35	<.001
Surp_S	unc005_k25	Unknown	32	62	24	3.218	1	34	<.001
Surp_S	unc005_k25	Left AnG angular gyrus	-42	-68	50	3.121	1	33	<.001
Surp_S	unc005_k25	Unknown	52	-70	-24	3.823	0.990	32	<.001
Surp_S	unc005_k25	Right MTG middle temporal gyrus	64	-30	-22	3.539	1	32	<.001
Surp_O	unc005_k25	Right TrIFG triangular part of the inferior frontal gyrus	44	28	0	3.550	0.998	71	0

S12. Full results of Pain intensity and Pain ratings

Pain intensity

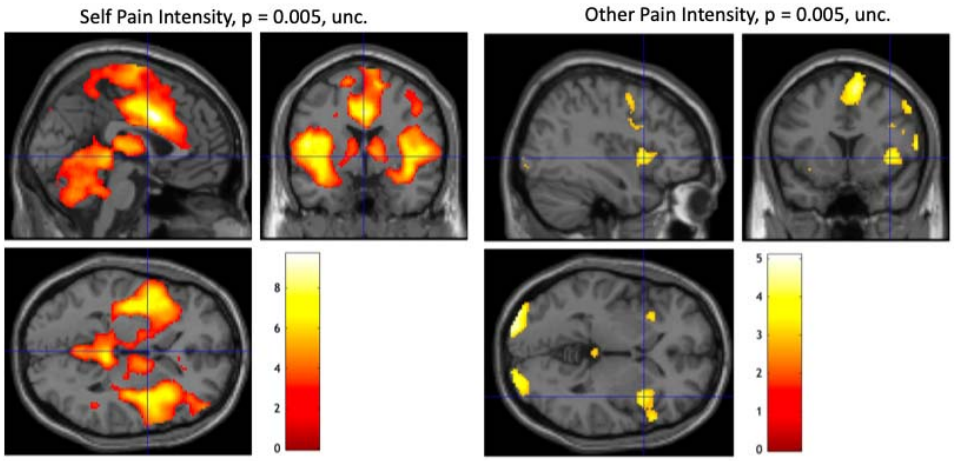

Figure S12.1. Pain intensity contrast maps for self and other

Table S12.1 Pain intensity univariate results in self and other

Contrast	Threshold	Region	X	Y	Z	peak_T	peak_pFWE	k_voxels	cluster_pFWE

Pain_S	FWE_p05	Left AIns anterior insula	-42	6	-6	8.880	<0.001	1780	NaN
Pain_S	FWE_p05	Right AIns anterior insula	36	8	8	7.881	0	1087	NaN
Pain_S	FWE_p05	Left MCgG middle cingulate gyrus	0	8	34	9.691	<0.001	891	NaN
Pain_S	FWE_p05	Left Cerebral White Matter	-54	-30	30	8.153	0	380	NaN
Pain_S	FWE_p05	Right PO parietal operculum	58	-28	26	7.387	0.001	297	NaN
Pain_S	FWE_p05	Left Cerebral White Matter	-8	-16	70	7.284	0.001	116	0
Pain_S	FWE_p05	Left SPL superior parietal lobule	-18	-48	66	6.839	0.003	86	0
Pain_S	FWE_p05	Unknown	6	-36	0	6.957	0.002	65	0
Pain_S	FWE_p05	Right Cerebral White Matter	14	-6	68	7.427	0.001	59	0
Pain_S	FWE_p05	Right Thalamus Proper	6	-10	6	6.248	0.013	29	0
Pain_S	FWE_p05	Right Cerebellum White Matter	20	-46	-48	6.740	0.004	21	0
Pain_S	FWE_p05	Right Thalamus Proper	4	-22	10	6.060	0.020	11	0
Pain_S	FWE_p05	Right TrIFG triangular part of the inferior frontal gyrus	46	38	6	6.199	0.015	9	0
Pain_S	FWE_p05	Right CO central operculum	56	-12	18	5.980	0.025	9	0
Pain_S	FWE_p05	Left Thalamus Proper	-8	-8	10	5.960	0.026	8	0
Pain_S	FWE_p05	Unknown	4	-8	78	5.723	0.045	1	<.001
Pain_S	unc005_k25	Left MCgG middle cingulate gyrus	0	8	34	9.691	4.276	42459	NaN
Pain_S	unc005_k25	Right PrG precentral gyrus	36	-6	52	4 4	0.908	265	0
Pain_S	unc005_k25	Right Cerebellum Exterior	32	-64	-22	3.944	0.933	168	0
Pain_S	unc005_k25	Left PrG precentral gyrus	-38	-8	48	4.274	0.736	162	0
Pain_S	unc005_k25	Left MTG middle temporal gyrus	-50	-62	8	4.334	0.689	143	0
Pain_S	unc005_k25	Left Cerebellum Exterior	-12	-54	-52	3.481	0.999	25	<0.001
Pain_O	unc005_k25	Unknown	62	14	12	4.288	0.718	674	0
Pain_O	unc005_k25	Right SMC supplementary	8	12	60	4.668	0.418	656	0

		motor cortex							
Pain_O	unc005_k25	Left IOG inferior occipital gyrus	-30	-98	2	4.762	0.354	469	0
Pain_O	unc005_k25	Right PrG precentral gyrus	50	4	50	5.086	0.186	433	0
Pain_O	unc005_k25	Right Cerebral White Matter	22	-96	-4	4.475	0.567	423	0
Pain_O	unc005_k25	Left Cerebellum Exterior	-34	-54	-30	4.013	0.898	172	0
Pain_O	unc005_k25	Right Cerebral White Matter	44	-2	32	3.277	1	140	0
Pain_O	unc005_k25	Brain Stem	6	-30	-24	3.393	1	43	0
Pain_O	unc005_k25	Left Cerebral White Matter	-34	-6	42	3.096	1	40	0
Pain_O	unc005_k25	Left SMG supramarginal gyrus	-62	-40	44	3.155	1	39	0
Pain_O	unc005_k25	Left Cerebral White Matter	-30	20	0	3.311	1	30	<0.001

Table S12.2 Pain ratings univariate results in self and other

Contrast	Threshold	Region	X	Y	Z	peak_T	peak_pFWE	k_voxels	cluster_pFWE
Ratings_S	unc005_k25	Right SPL superior parietal lobule	10	-68	54	5.114	0.199	845	0
Ratings_S	unc005_k25	Right MFG middle frontal gyrus	28	8	58	4.614	0.506	247	0
Ratings_S	unc005_k25	Right PrG precentral gyrus	40	4	32	3.452	1	184	0
Ratings_S	unc005_k25	Left Cerebellum Exterior	-52	-62	-42	3.810	0.982	129	0
Ratings_S	unc005_k25	Right MFG middle frontal gyrus	46	48	14	3.877	0.970	115	0
Ratings_S	unc005_k25	Right SMC supplementary motor cortex	4	14	58	3.299	1	111	0
Ratings_S	unc005_k25	Unknown	50	6	54	3.399	1	79	0
Ratings_S	unc005_k25	Right SMG supramarginal gyrus	54	-38	52	3.353	1	60	0
Ratings_S	unc005_k25	Right Cerebral White Matter	32	40	-4	3.464	1	32	<0.001
Ratings_S	unc005_k25	Unknown	-44	-78	-26	3.423	1	26	<0.001
Ratings_O	unc005_k25	Right SFG superior frontal gyrus	24	10	64	4.826	0.406	1220	0
Ratings_O	unc005_k25	Right MFG	44	28	38	5.233	0.183	463	0

		middle frontal gyrus							
Ratings_O	unc005_k25	Right SMG supramarginal gyrus	52	-38	52	5.012	0.287	382	0
Ratings_O	unc005_k25	Left MFG middle frontal gyrus	-28	6	64	3.760	0.995	353	0
Ratings_O	unc005_k25	Left Cerebellum Exterior	-44	-64	-36	4.109	0.924	167	0
Ratings_O	unc005_k25	Left Cerebral White Matter	-44	-50	42	3.441	1	134	0
Ratings_O	unc005_k25	Left SPL superior parietal lobule	-24	-70	54	4.276	0.834	124	0
Ratings_O	unc005_k25	Right MFG middle frontal gyrus	42	50	6	4.041	0.949	121	0
Ratings_O	unc005_k25	Right Cerebral White Matter	42	-46	38	3.587	0.999	78	0
Ratings_O	unc005_k25	Right Cerebellum Exterior	44	-70	-28	3.310	1	46	0
Ratings_O	unc005_k25	Right PCu precuneus	6	-70	46	3.801	0.992	39	0
Ratings_O	unc005_k25	Left MTG middle temporal gyrus	-52	-42	0	2.980	1	29	<0.001
Ratings_O	unc005_k25	Right TrIFG triangular part of the inferior frontal gyrus	46	44	-4	3.503	1	26	<0.001

A)

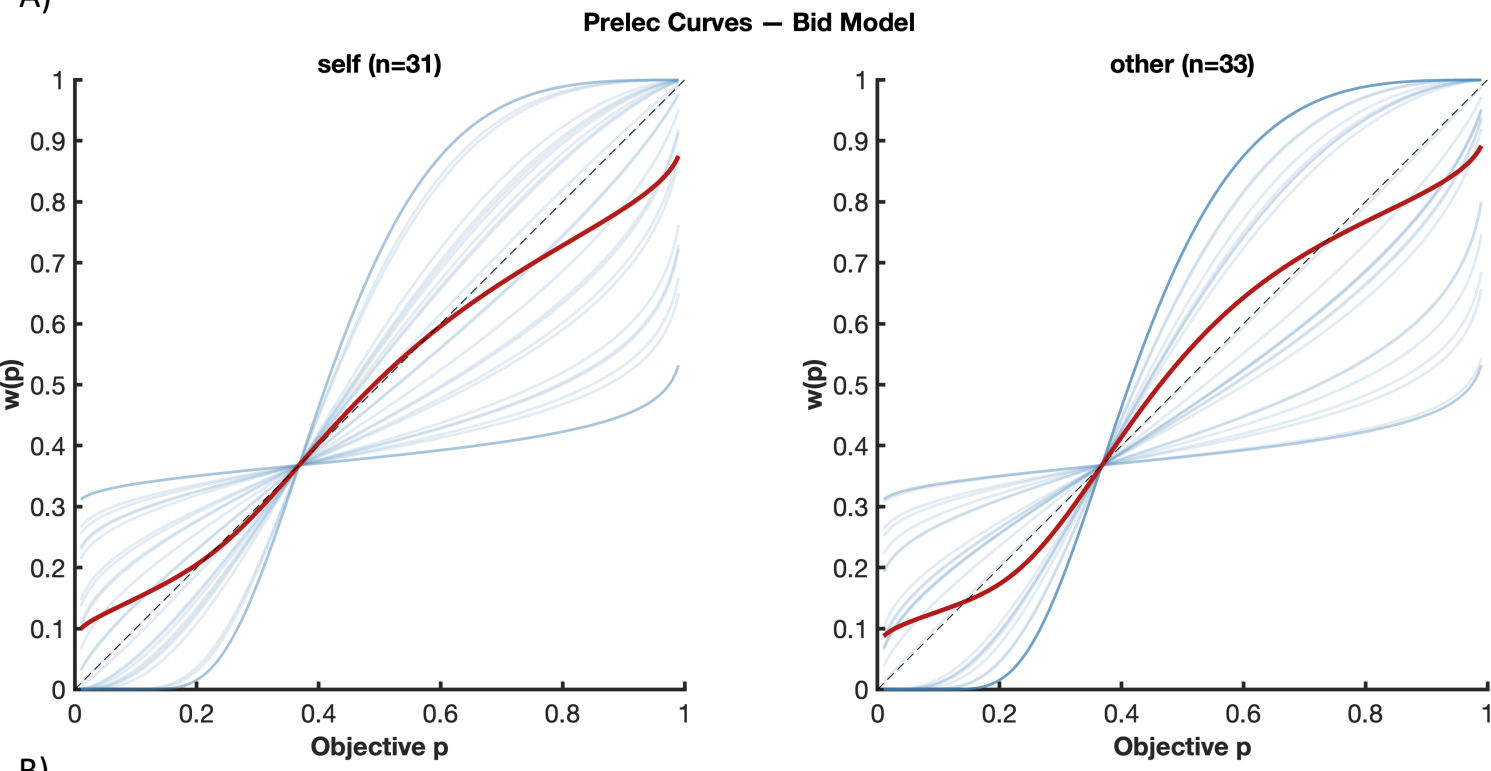
Prelec Curves — Bid Model
self (n=31)
other (n=33)
w(p)
Objective p
0
0.1
0.2
0.3
0.4
0.5
0.6
0.7
0.8
0.9
1
0.2
0.4
0.6
0.8

B)

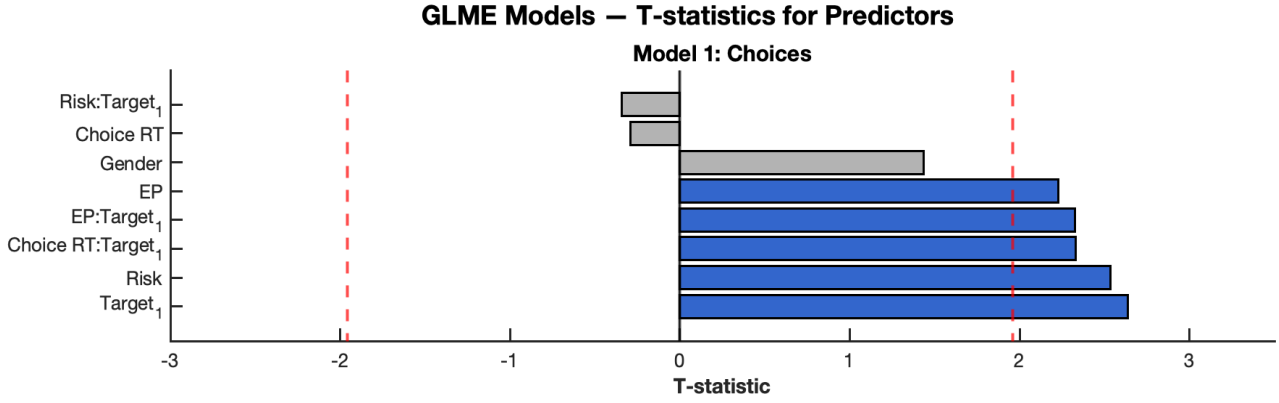
GLME Models — T-statistics for Predictors
Model 1: Choices
Risk:Target1
Choice RT
Gender
EP
EP:Target1
Choice RT:Target1
Risk
Target1
-3
-2
-1
0
1
2
3
T-statistic

C)

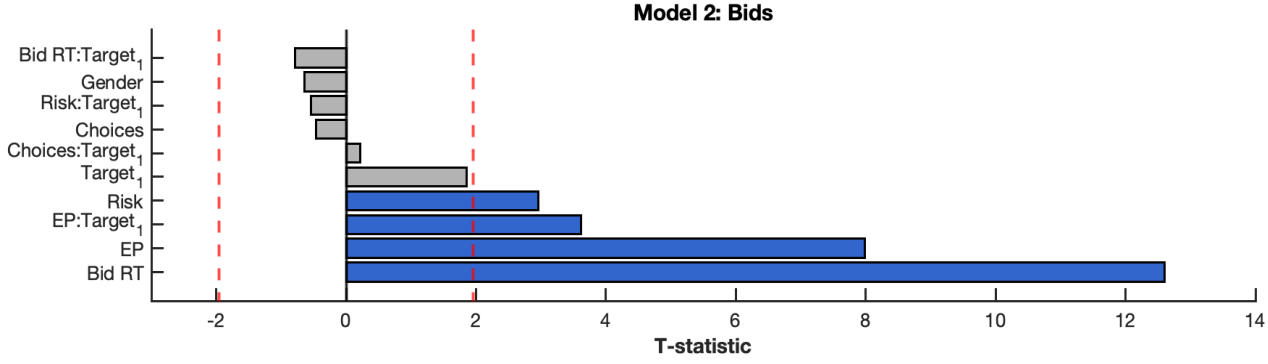
Model 2: Bids
Bid RT:Target1
Gender
Risk:Target1
Choices
Choices:Target1
Target1
Risk
EP:Target1
EP
Bid RT
-2
0
2
4
6
8
10
12
14
T-statistic

D)

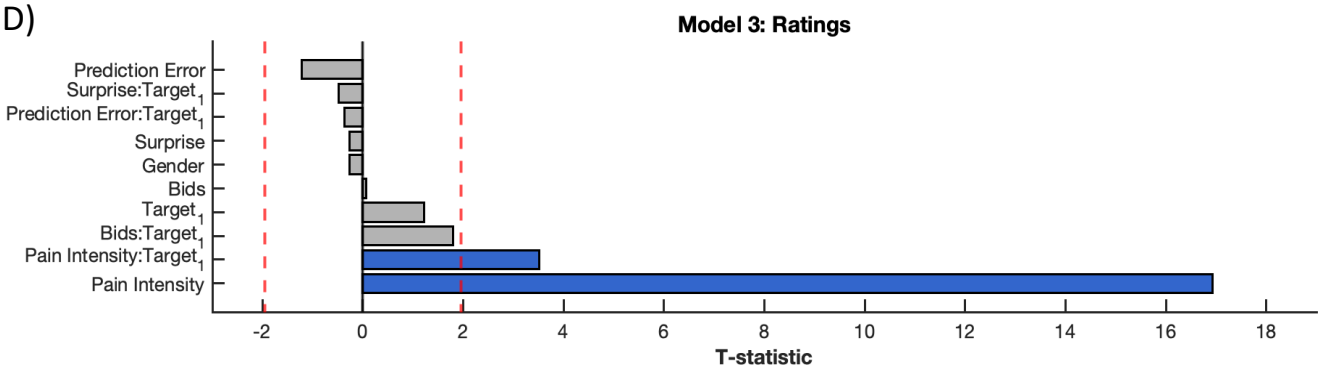
Model 3: Ratings
Prediction Error
Surprise:Target1
Prediction Error:Target1
Surprise
Gender
Bids
Target1
Bids:Target1
Pain Intensity:Target1
Pain Intensity
-2
0
2
4
6
8
10
12
14
16
18
T-statistic

Figure 2. Expected Pain and Risk (Predictive Phase)

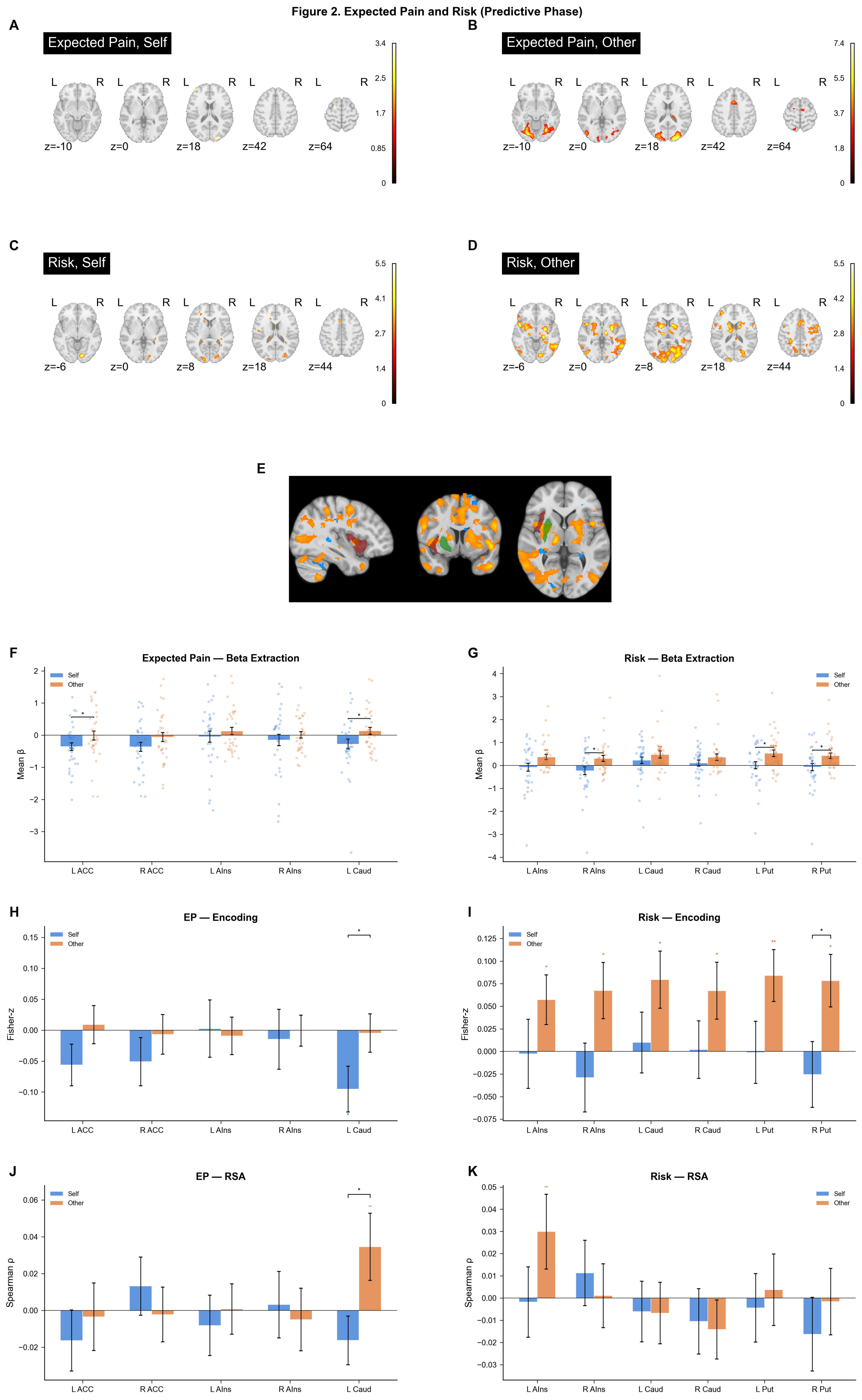

Figure 3. Prediction Error and Surprise (Post-Outcome Phase)

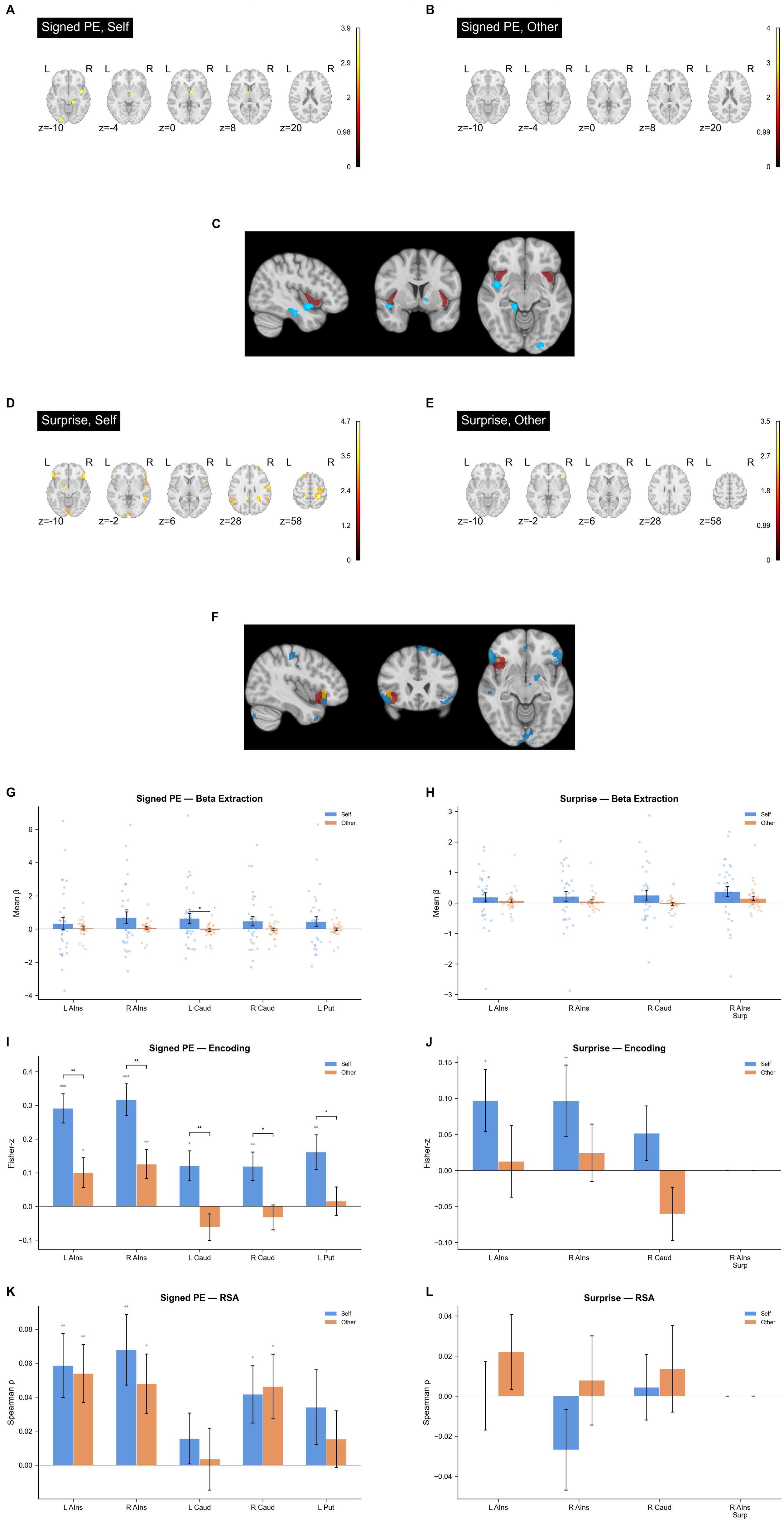

A

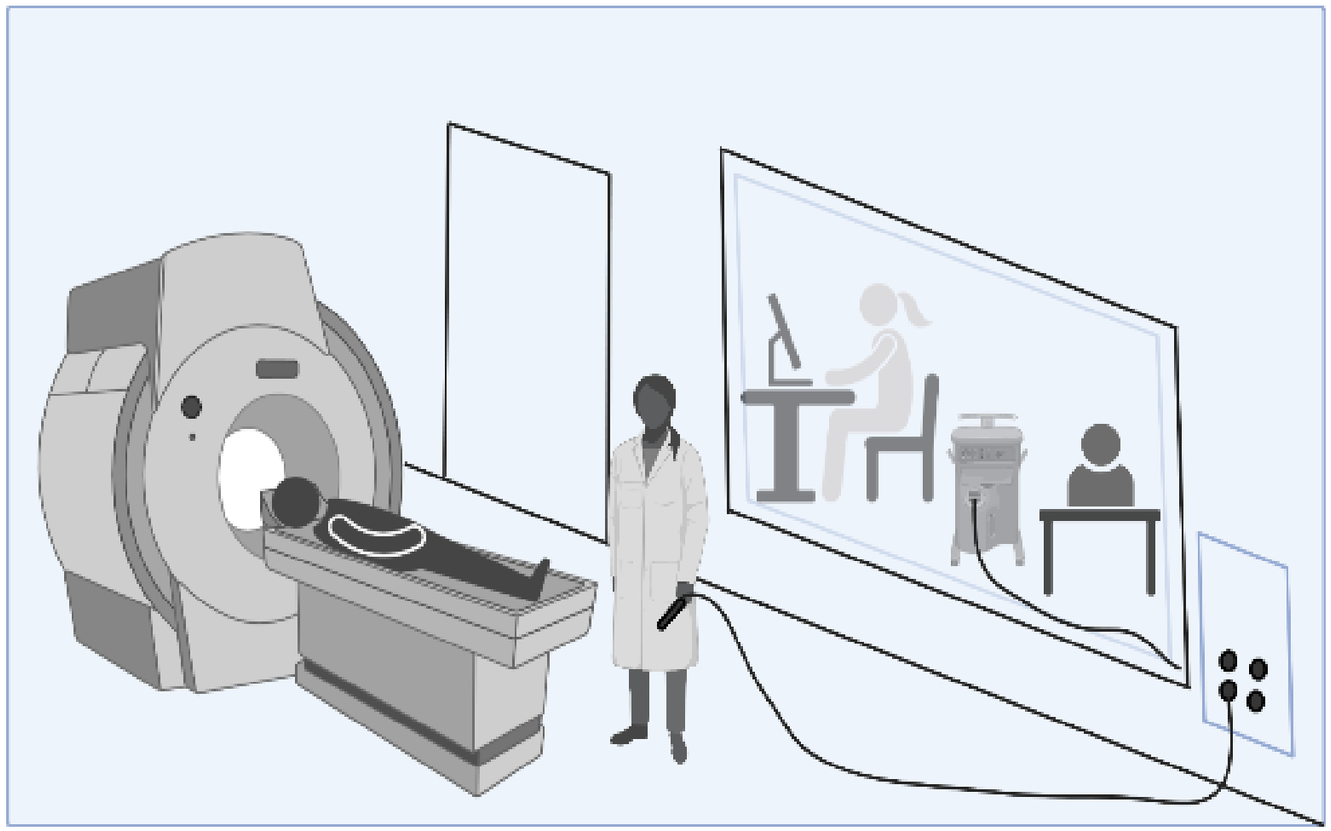

B

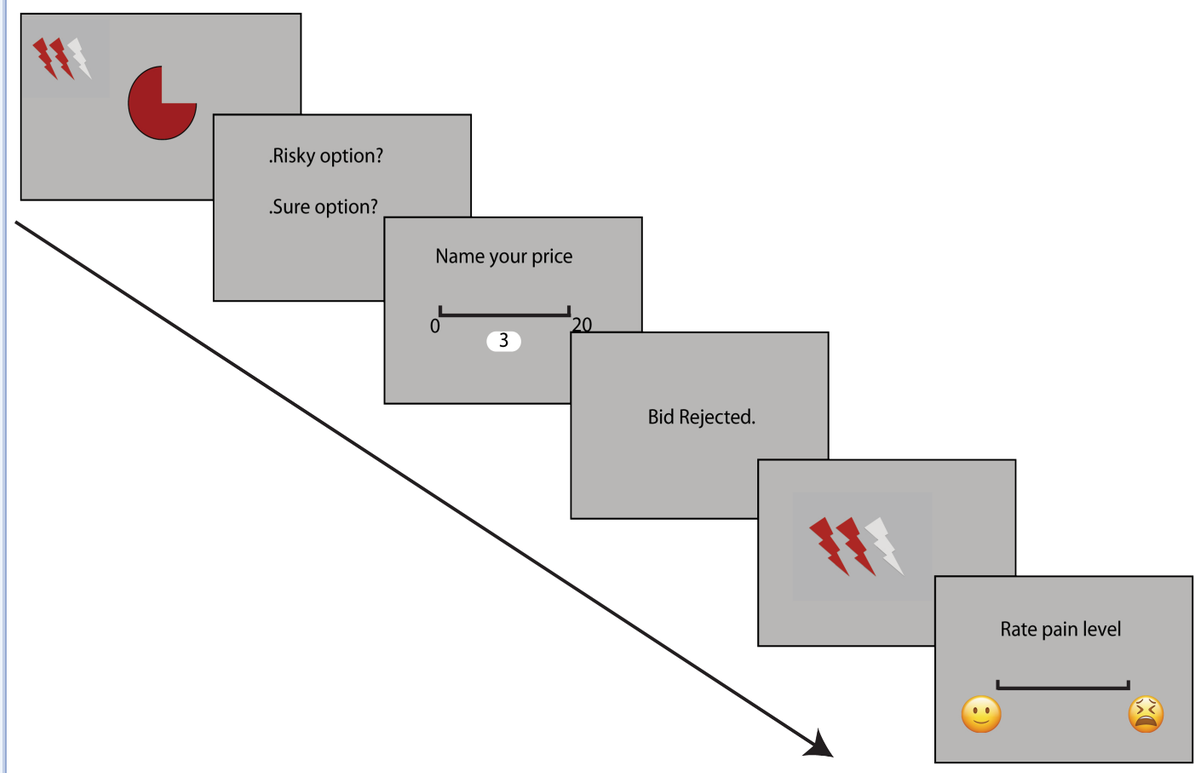
.Risky option?
.Sure option?
Name your price
0
3
20
Bid Rejected.
Rate pain level

C

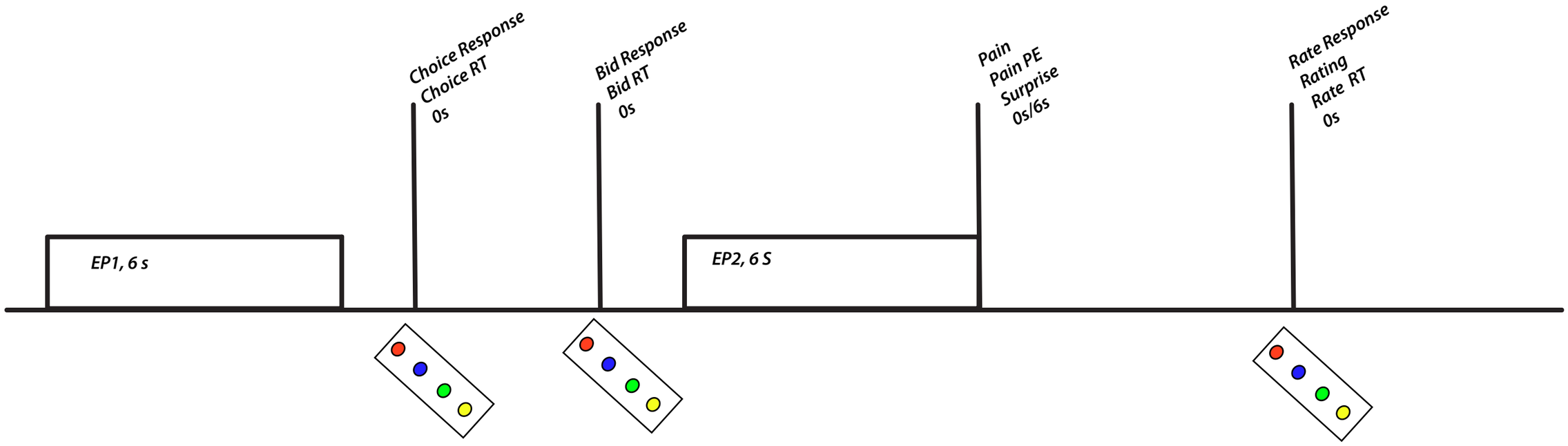
Choice Response
Choice RT
0s
Bid Response
Bid RT
0s
Pain
Pain PE
Surprise
0s/6s
Rate Response
Rating
Rate RT
0s
EP1, 6 s
EP2, 6 S